National School on Neutron and X-ray Scattering
August 15-29, 2004
Argonne National Laboratory

^^

Magnetic Scattering II: Applications

C.F.Majkrzak

National Institute of Standards and Technology

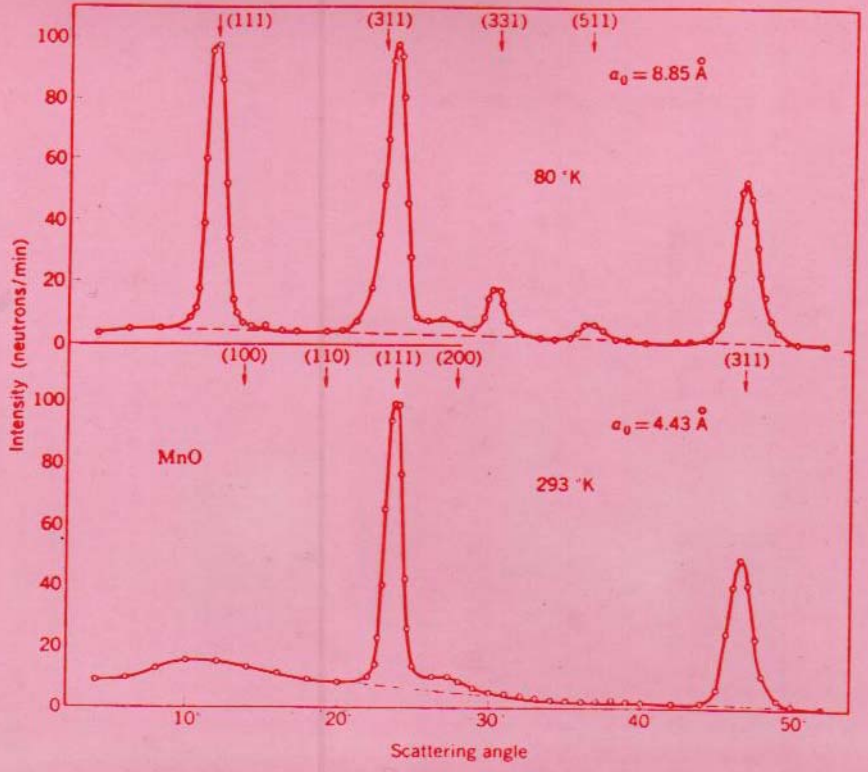

Figure 23 Neutron diffraction patterns for MnO below and above the spin-ordering temperature of 120°K, after C. G. Shull, W. A. Strauser, and E. O. Wollan. Phys. Rev. 83, 333 (1951). The reflection indices are based on an 8.85 Å cell at 80°K and on a 4.43 Å cell at 293°K. At the higher temperature the Mn^{2+} ions are still magnetic, but they are no longer ordered.

ANTIFERROMAGNETIC ORDER

A classical example of magnetic structure determination by neutrons is shown in Fig. 23 for MnO, which has the NaCl structure. At 80°K there are extra neutron reflections not present at 293°K. The reflections at 80°K may be classified in terms of a cubic unit cell of lattice constant 8.85 Å. At 293°K the reflections correspond to an fcc unit cell of lattice constant 4.43 Å. But the lattice constant determined by x-ray reflection is 4.43 Å at *both* temperatures, 80°K and 293°K. We conclude that the chemical unit cell has the 4.43 Å lattice parameter, but that at 80°K the electronic magnetic moments of the Mn^{2+} ions are ordered in some nonferromagnetic arrangement. If the ordering were ferromagnetic, the chemical and magnetic cells would give the same reflections. The spin arrangement shown in Fig. 24 is consistent with the neutron diffraction results and with magnetic measurements. The spins in a single [111] plane are parallel, but adjacent [111] planes are antiparallel. Thus MnO is an antiferromagnet, as in Fig. 25.

(KITTEL)

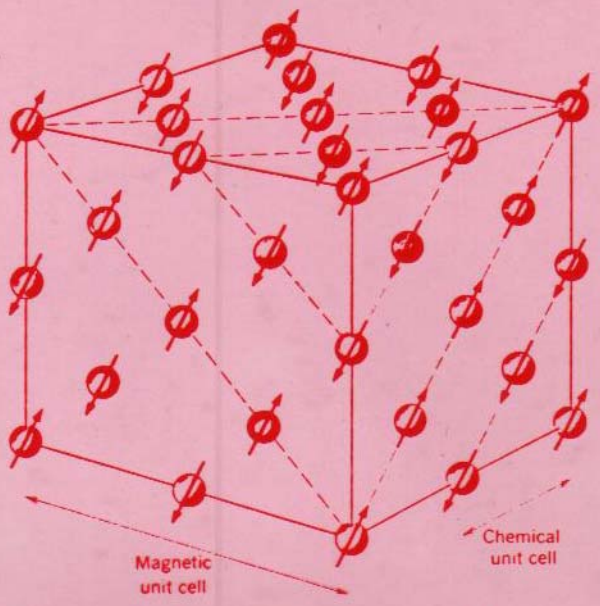

Figure 24 Ordered arrangements of spins of the Mn^{2+} ions in manganese oxide, MnO, as determined by neutron diffraction. The O^{2-} ions are not shown.

Figure 25 Spin ordering in ferromagnets ($J > 0$) and antiferromagnets ($J < 0$).

(KITTEL)

- X-RAY SCATTERING LENGTH (FOR CHARGE SCATTERING) IS Q-DEPENDENT DUE TO SPATIAL EXTENT OF ATOM'S ELECTRON DISTRIBUTION — Q-DEPENDENCE OF SCATTERING LENGTH IS DESCRIBED BY A "FORM" FACTOR

- NEUTRON SCATTERING LENGTH (FOR MAGNETIC SCATTERING) IS ALSO Q-DEPENDENT DUE TO SPATIAL EXTENT OF ATOM'S UNPAIRED ELECTRON DISTRIBUTION — Q-DEPENDENCE IS CHARACTERIZED BY A MAGNETIC "FORM" FACTOR

- BOTH ORBITAL AND SPIN MOMENTS OF UNPAIRED ELECTRONS IN CRYSTALS CONTRIBUTE TO THE MAGNETIZATION DENSITY $M(\vec{r})$; THE MAGNETIC FORM FACTOR IS

$$f(\vec{Q}) = \frac{\iiint M(\vec{r}) e^{i\vec{Q}\cdot\vec{r}} d\vec{r}^3}{\iiint M(\vec{r}) d\vec{r}^3}$$

- MAGNETIC SCATTERING LENGTH FOR NEUTRONS IS

$$p \propto \mu f(\vec{Q})$$

WHERE μ IS THE EFFECTIVE ATOMIC MAGNETIC MOMENT

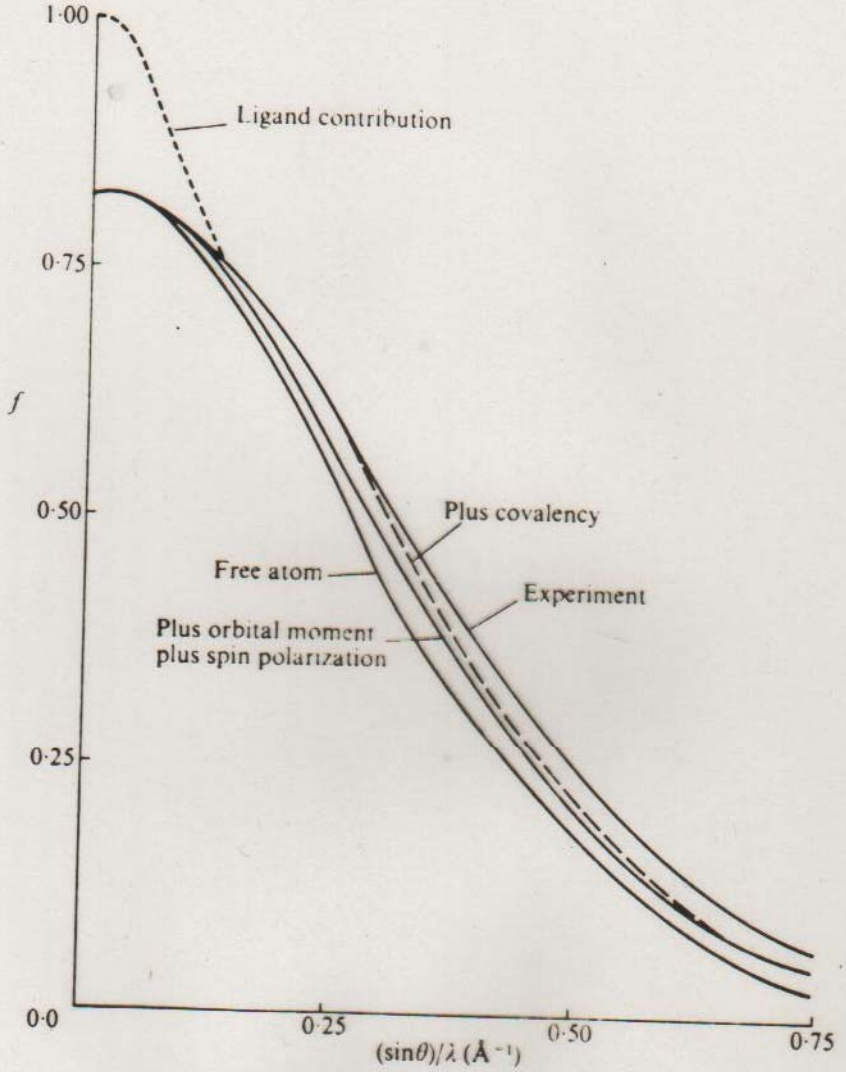

FIG. 151. Experimental and theoretical form factors for NiO.

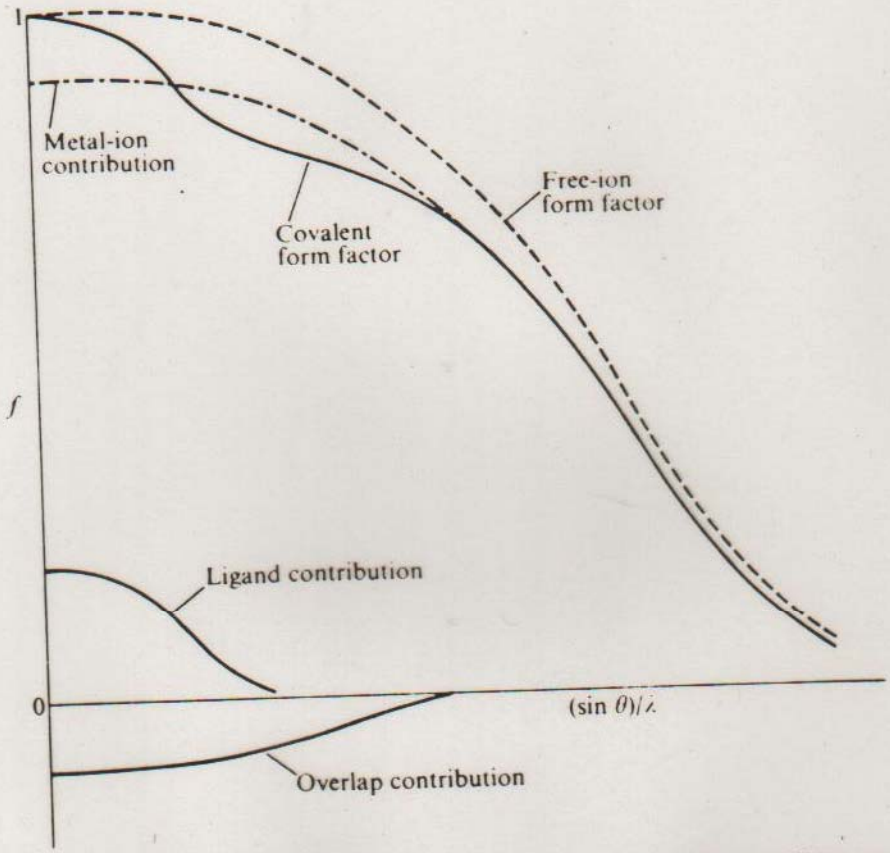

FIG. 152. The three contributions to the form-factor curve of an antiferromagnet: the reduced metal ion contribution, a negative overlap term, and (for asymmetrical structures) a ligand contribution. (Rimmer 1970.)

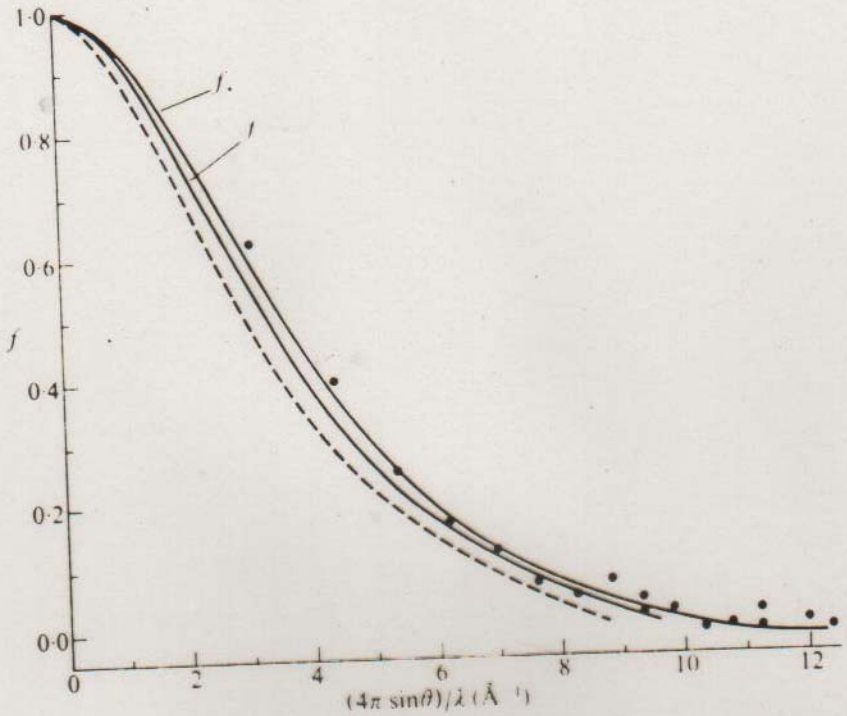

FIG. 126. Magnetic form factor curves for iron. The full-line curves show the calculation by Wood and Pratt for, respectively, the five 3d electrons of +ve spin and the single 3d electron of −ve spin for a free iron atom. The points are the experimental measurements of Shull and Yamada for metallic iron. The broken-line curve contrasts the experimental data for the Fe^{3+} ion in magnetite.

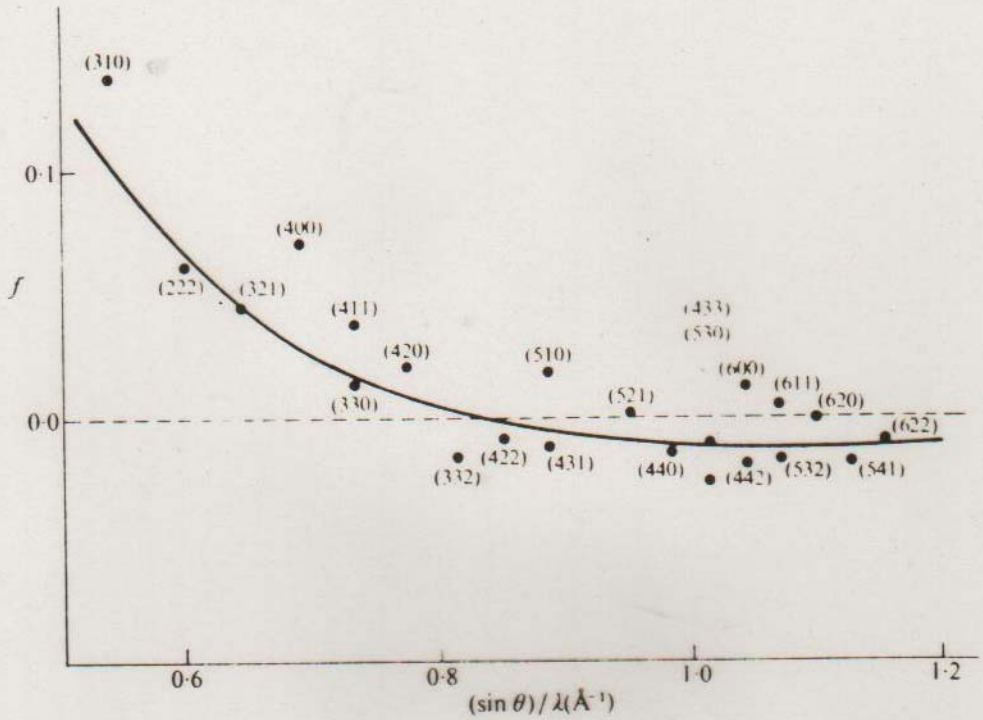

FIG. 131. The high-angle portion of the Shull and Yamada form-factor data for metallic iron, emphasizing the differences between five pairs of reflections with the same value of scattering angle.

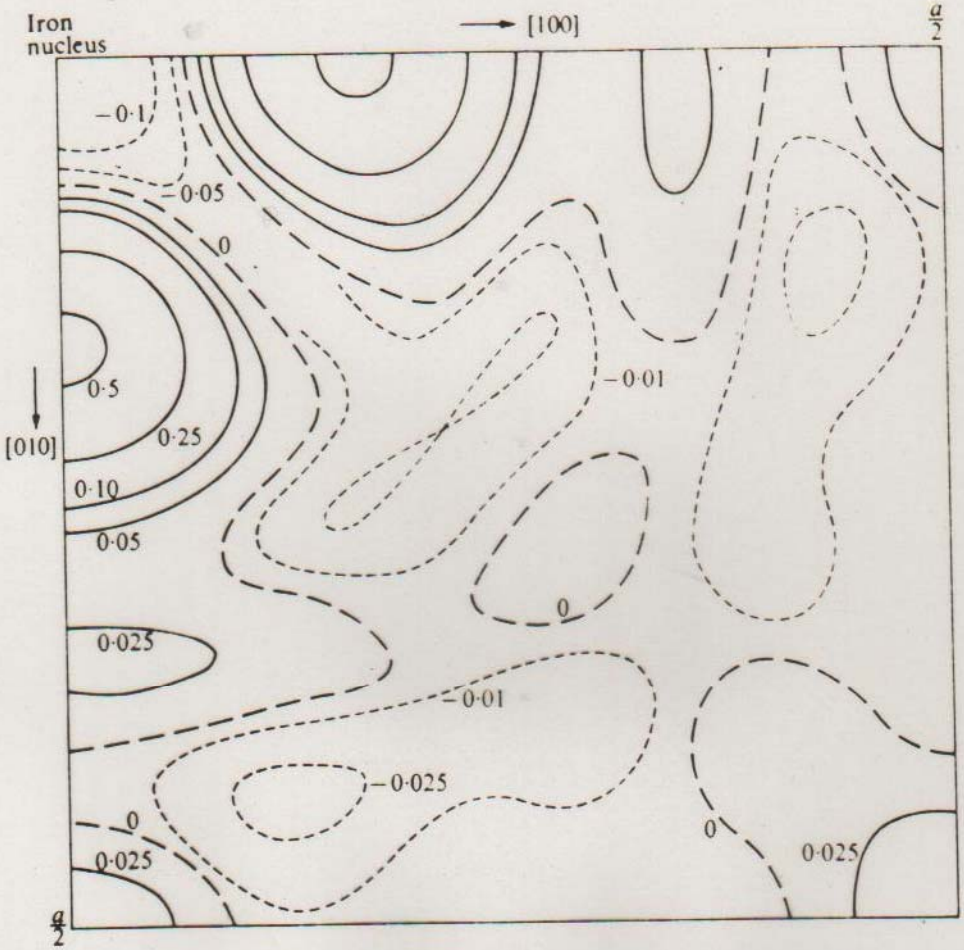

FIG. 133. A plot of the excess spin density in iron, measured experimentally, compared with that expected for a spherically symmetrical free atom. Contours are in units of μ_B Å^{-3}. (Shull and Yamada 1962.)

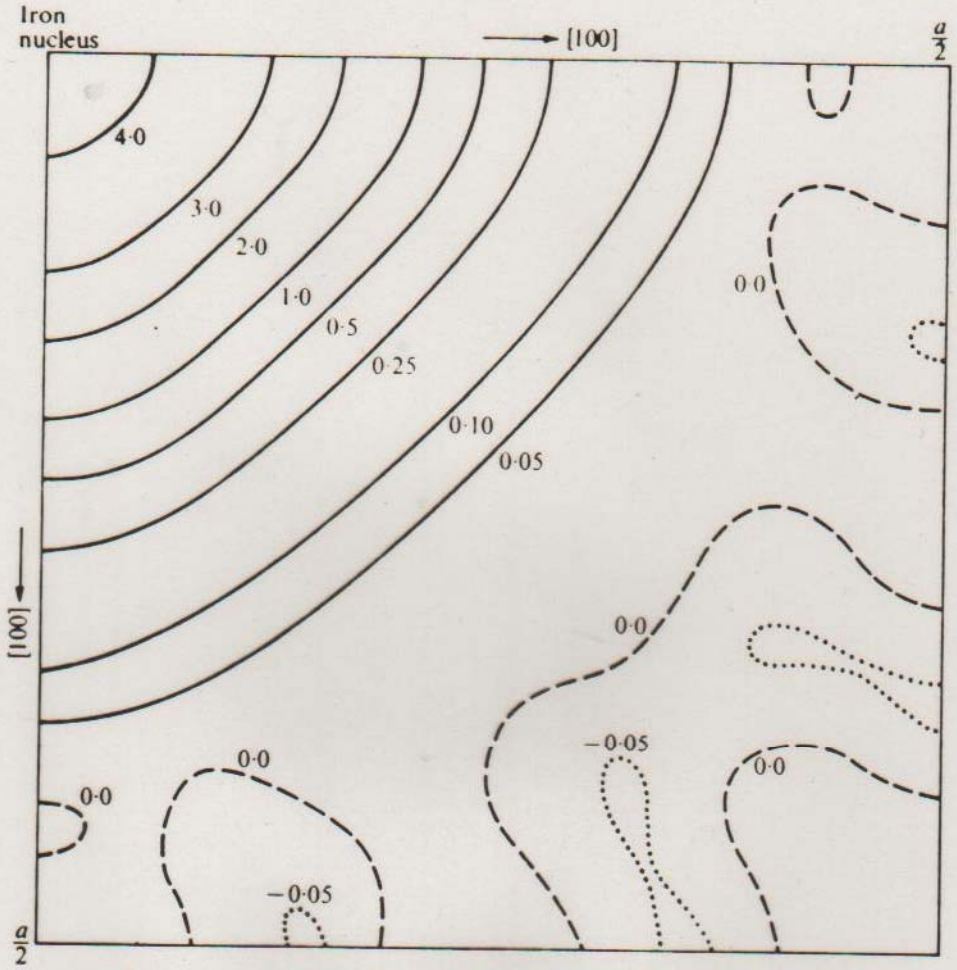

FIG. 132. A plot of the spin-density distribution in the (100) plane of iron, indicating an excess along the [100] axis relative to that along [110]. Contours are in units of μ_B Å^{-3}. (Shull and Yamada 1962.)

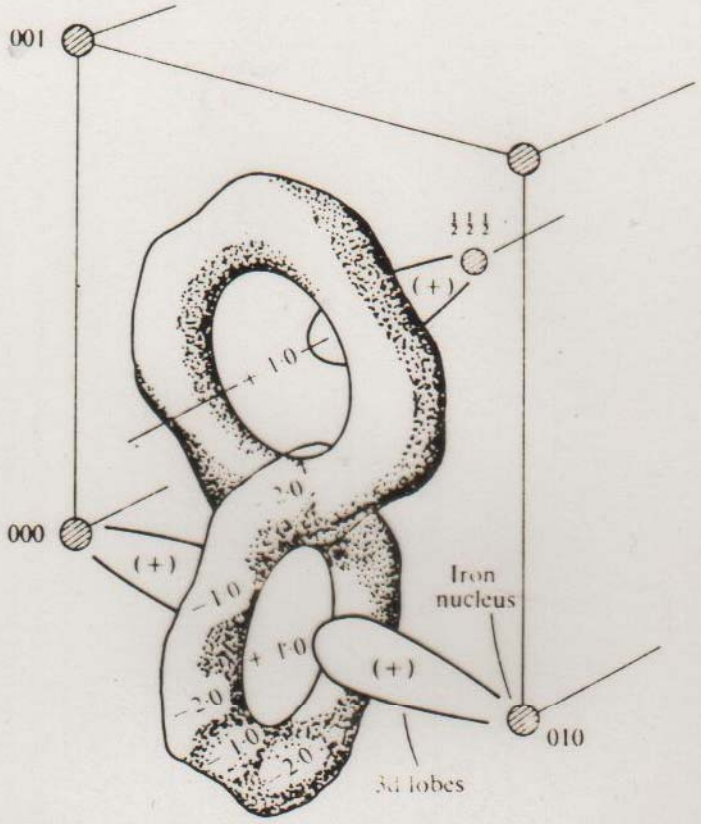

FIG. 134. The residual magnetization (kG) in iron as deduced experimentally by Shull and Mook (1966). The positive excess of 3d magnetization along the cube edges is over-emphasized in comparison with the interlocking rings of negative magnetization. The rings shown are centred on $0\frac{1}{2}0$, $0\frac{1}{2}\frac{1}{2}$.

compounds, but it became evident, as more precise experimental data became available, that significant differences exist. Early measurements related to the ions Fe^{3+}, Mn^{2+}, and Ni^{2+}, and it appeared that for the ions Fe^{3+} and Mn^{2+} in a crystal the spin density was more diffuse than that calculated for a free atom, but that for the ion Ni^{2+} the reverse was the case; for the latter ion the observed form-factor curve was broader than expected.

In our subsequent study of the form factors of the metals themselves we have shown that precise measurements with polarized neutrons have revealed angular dependencies in the form-factor curve which could be correlated with the details of the electronic distribution. Ionic compounds which show co-operative magnetism are generally antiferromagnetic, and the quantitative study of their atomic form factors is much more difficult. However, it became evident in the 1960s that a number of discrepancies existed. The most outstanding discovery was that of Nathans *et al.* (1963), who observed magnetic scattering in forbidden directions in MnF_2. This and other observations can be accounted for by the assumption that these salts are not completely ionic but show a certain amount of covalency. Thus some part of the electronic charge, which in an ideal ionic bond is completely transferred from cation to anion, is returned to the cation. In the case of a magnetic material there is a transfer of electron spin. We shall see that this can result in modification both of the observed form factors and the observed magnetic intensities.

The principle involved in this discussion is illustrated in Fig. 149, which relates to a magnetic salt constituted of a magnetic cation and an anion such as O^{2-} or F^-. For an ideal ionic bond there

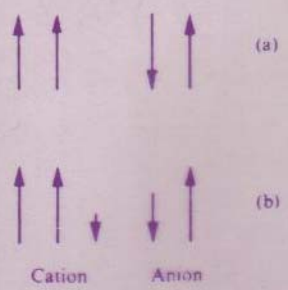

FIG. 149. Transfer of electron charge from anion to cation in covalent bond (b). For an ideal ionic bond (a) there will be no unpaired spin density on the anion.

Spin and Orbital Magnetic Moments of Fe_3O_4

D. J. Huang,[1,2] C. F. Chang,[1] H.-T. Jeng,[3] G. Y. Guo,[4,1] H.-J. Lin,[1] W. B. Wu,[2,1] H. C. Ku,[5] A. Fujimori,[6] Y. Takahashi,[7] and C. T. Chen[1]

[1]*National Synchrotron Radiation Research Center, Hsinchu 30077, Taiwan*
[2]*Department of Electrophysics, National Chiao-Tung University, Hsinchu 300, Taiwan*
[3]*Physics Division, National Center for Theoretical Sciences, Hinchu 300, Taiwan*
[4]*Department of Physics, National Taiwan University, Taipei 106, Taiwan*
[5]*Department of Physics, National Tsing Hua University, Hsinchu 300, Taiwan*
[6]*Department of Complexity Science and Engineering and Department of Physics, University of Tokyo, Tokyo 113-0033, Japan*
[7]*Graduate School and Faculty of Science, Himeji Institute of Technology, Hyogo 678-1297, Japan*

(Received 9 January 2004; published 11 August 2004)

We present measurements of the spin and orbital magnetic moments of Fe_3O_4 by using SQUID and magnetic circular dichroism in soft x-ray absorption. The measurements show that Fe_3O_4 has a noninteger spin moment, in contrast to its predicted half-metallic feature. Fe_3O_4 also exhibits a large unquenched orbital moment. Calculations using the local density approximation including the Hubbard U method and the configuration interaction cluster-model suggest that strong correlations and spin-orbit interaction of the $3d$ electrons result in the noninteger spin and large orbital moments of Fe_3O_4.

DOI: 10.1103/PhysRevLett.93.077204 PACS numbers: 75.50.Ss, 71.28.+d, 75.25.+z, 78.70.Dm

Magnetite (Fe_3O_4) exhibits many interesting properties such as charge ordering, mixed valence, and metal-insulator transition known as the Verwey transition [1], in which the conductivity decreases by 2 orders of magnitude upon cooling through the transition temperature $T_V \sim 120$ K. In spite of intensive studies on its electronic structure, surprisingly, no consensus has been reached concerning the electronic nature of Fe_3O_4. Experimental studies, including neutron diffuse scattering [2], NMR [3], and x-ray scattering [4,5], indicate that Fe_3O_4 should be considered as an itinerant magnet rather than a fluctuating mixed-valence material. According to band theory, Fe_3O_4 is a half-metal above T_V; its minority-spin electrons are conducting, whereas the majority-spin ones are insulating [6]. In addition, Fe_3O_4 would have an integral spin moment per formula unit (f.u.), i.e., $4.0\mu_B$; the orbital moment of metallic Fe_3O_4 would be quenched.

On the other hand, charge ordering of the octahedral (B-site) Fe in Fe_3O_4 has been suggested by the refinements of x-ray and neutron diffraction data [7], implying that the $3d$ electrons of Fe_3O_4 have a strong localized character. Fe^{2+} in Fe_3O_4 is thus expected to exhibit a large unquenched orbital moment, like Fe^{2+} in FeO [8]. Theoretical and experimental works show that localization of the $3d$ electrons of transition-metal compounds leads to giant orbital moments. For example, FeO [8], CoO [9], Fe impurities in alkali metals [10], and Fe nitridometalates [11] are shown to have giant or unquenched orbital moments. In addition, calculations based on atomic multiplet theory show that the localized nature of the open $3d$ shell of Fe_3O_4 sets a limit of -66.7% on the spin polarization of conduction electrons [12], rather than -100% predicted by band theory. Results of spin-resolved photoemission from epitaxial thin films and single crystals of Fe_3O_4 support the conclusion of multiplet calculations [13–16], in contrast to the conclusion from spin-resolved photoemission of $Fe_3O_4(111)$ thin films grown on W(110) [17].

Measurements of orbital and spin moments therefore provide an opportunity to explore the character of $3d$ electrons in Fe_3O_4 [18,19]. Examining whether Fe_3O_4 has a quenched orbital moment and an integral spin moment is important in revealing its electronic nature.

In this Letter, we present studies of the spin and orbital moments of Fe_3O_4 single crystals by combining magnetic circular dichroism (MCD) in soft x-ray absorption spectroscopy (XAS) and measurements using a superconducting quantum interference device (SQUID) magnetometer. In addition, we performed cluster-model calculations in the configuration interaction (CI) approach and band-structure calculations in the local spin density approximation including the on-site Coulomb interaction U (LDA + U) [20,21] to unravel the underlying physics of the magnetic moments of Fe_3O_4.

Single crystals of Fe_3O_4 were grown by the floating zone method and fully characterized by x-ray diffraction. Temperature-dependent measurements of the resistance of the crystal show an abrupt change at 120 K, as plotted in Fig. 3(a), revealing the Verwey transition of Fe_3O_4. We measured the total magnetic moment of a 21.59-mg Fe_3O_4 single crystal with an applied field of 1 T along the [111] direction using a SQUID magnetometer.

We measured MCD in XAS on Fe_3O_4 at various temperatures under an applied magnetic field of 1 T along the [111] direction using the Dragon beam line at the National Synchrotron Radiation Research Center in Taiwan. XAS spectra of Fe_3O_4 were taken in the total electron yield (TEY) mode with a photon-energy resolution of 0.2 eV

 0031-9007/04/93(7)/077204(4)$22.50

Research in Nanomagnetism at the NCNR

Ferromagnetic semiconductors:

Materials - GaMnAs/GaAs and EuS/PbS multilayers, $CoTiO_2$ films
Collaborators - Univ. Warsaw, Oregon State, Univ. Utah, Univ. Missouri, Purdue Univ., IBM, Indiana Univ., Ohio Univ.

Exchange-biased layers:

Materials - Fe_3O_4/CoO and Fe_3O_4/NiO superlattices, Fe/PdMn, Fe/FeF_2 and Co/FeMn bilayers
Collaborators —Philips Laboratory, Florida State, IBM, UCSD, Michigan State, William and Mary, LANSCE

Exchange Springs:

Materials - CoFe/FePt and Fe/Fe_3O_4 bilayers
Collaborators – IBM, NIST (Metallurgy Division)

Tunnel junctions:

Materials - Co/SiO_2 granular films and multilayers
Collaborators - Center for Magnetic Recording Research at UCSD

Magnetic storage media:

Materials - AFC media, Granular magnetic media
Collaborators - IBM

Magnetic nanoparticles:

Materials - Nanoparticles in a self-assembled polymer matrix
Collaborators - Univ. Maryland, NIST (Metallurgy Division)

Magnetic coupled layers:

Materials - GMR multilayers, Oxide-based CMR layers
Collaborators - Michigan State Univ., Univ. Maryland

NEUTRON REFLECTIVITY STUDIES OF MAGNETIC MULTILAYERS

C.F.Majkrzak (National Institute of Standards and Technology, USA)

Historically, neutron elastic scattering studies have provided a wealth of important atomic scale information about the magnetic structures of condensed matter, a significant part of which could not have been obtained by any other means. In the beginning, magnetic neutron diffraction research was performed primarily on bulk crystals. In more recent years, advances in thin film deposition techniques have made it possible to synthesize a variety of new types of layered magnetic systems, with properties that can be tailored for studies of fundamental scientific interest as well as technological applications. Throughout this still ongoing development, neutron scattering techniques, especially polarized neutron reflectometry (PNR) and diffraction, have made and continue to make significant contributions to the understanding of the physical behavior of magnetic thin films and superlattices (see, for example, references [1,2]).

Polarized neutron reflectometry can be divided into two broad categories, one of which corresponds to reflection measurements performed with the wavevector transfer Q normal to the film surface, commonly referred to as specular reflectometry, and the other to scattering done with some component of Q lying in the plane of the film. Analysis of the specular polarized neutron reflectivity, measured as a function of Q, yields the in-plane average of the vector magnetization depth profile along the surface normal, with a spatial resolution of less than a nanometer in certain cases. The nonspecular reflectivity, on the other hand, reveals in-plane magnetic structure, such as that associated with domains or artificially patterned surfaces. In this presentation, we will first briefly review what exactly makes PNR such an extraordinarily sensitive, and in some regards unique, probe of magnetic order in thin films and multilayers. We will also summarize the present state-of-the-art and new developments in experimental and theoretical PNR methods (for example, [3]).

In the second part of the talk, we will discuss current relevant applications of PNR, including the study of giant magneto-resistance (GMR) film sandwiches and magnetic semiconductor films and superlattices [4], of particular interest to the relatively new field of "spintronics".

References

1. C.F.Majkrzak, J.Kwo, M.Hong, Y.Yafet, D.Gibbs, C.L.Chien, and J.Bohr, Advances in Physics **40**, 99 (1991).
2. M.R.Fitzsimmons, S.D.Bader, J.A.Borchers, G.P.Felcher, J.K.Furdyna, A.Hoffmann, J.B.Kortright, I.K.Schuller, T.C.Schulthess, S.K.Sinha, M.F.Toney, D.Weller, and S.Wolf, Journal of Magnetism and Magnetic Materials, in press.
3. K.V.O'Donovan, J.A.Borchers, C.F.Majkrzak, O.Hellwig, and E.E.Fullerton, Physical Review Letters **88**, 672011(2002).
4. H.Kepa, G.Springholz, T.M.Giebultowicz, K.I.Goldman, C.F.Majkrzak, P.Kacman, J.Blinkowski, S.Holl, H.Krenn, and G.Bauer, Physical Review B, in press.

SUPERLATTICES (MBE)

MAGNETIC	ELECTRONIC	PROTONIC & NUCL
COLLINEAR NONCOLLINEAR FM, AFM, FERRI, LOCALIZED ITINERANT (Fe, Ni, Cr, Co, REs)	INSULATOR SEMICONDUCTOR CONDUCTOR SUPERCONDUCTOR	PRESENCE OF H NUCLEAR ORDER (SP

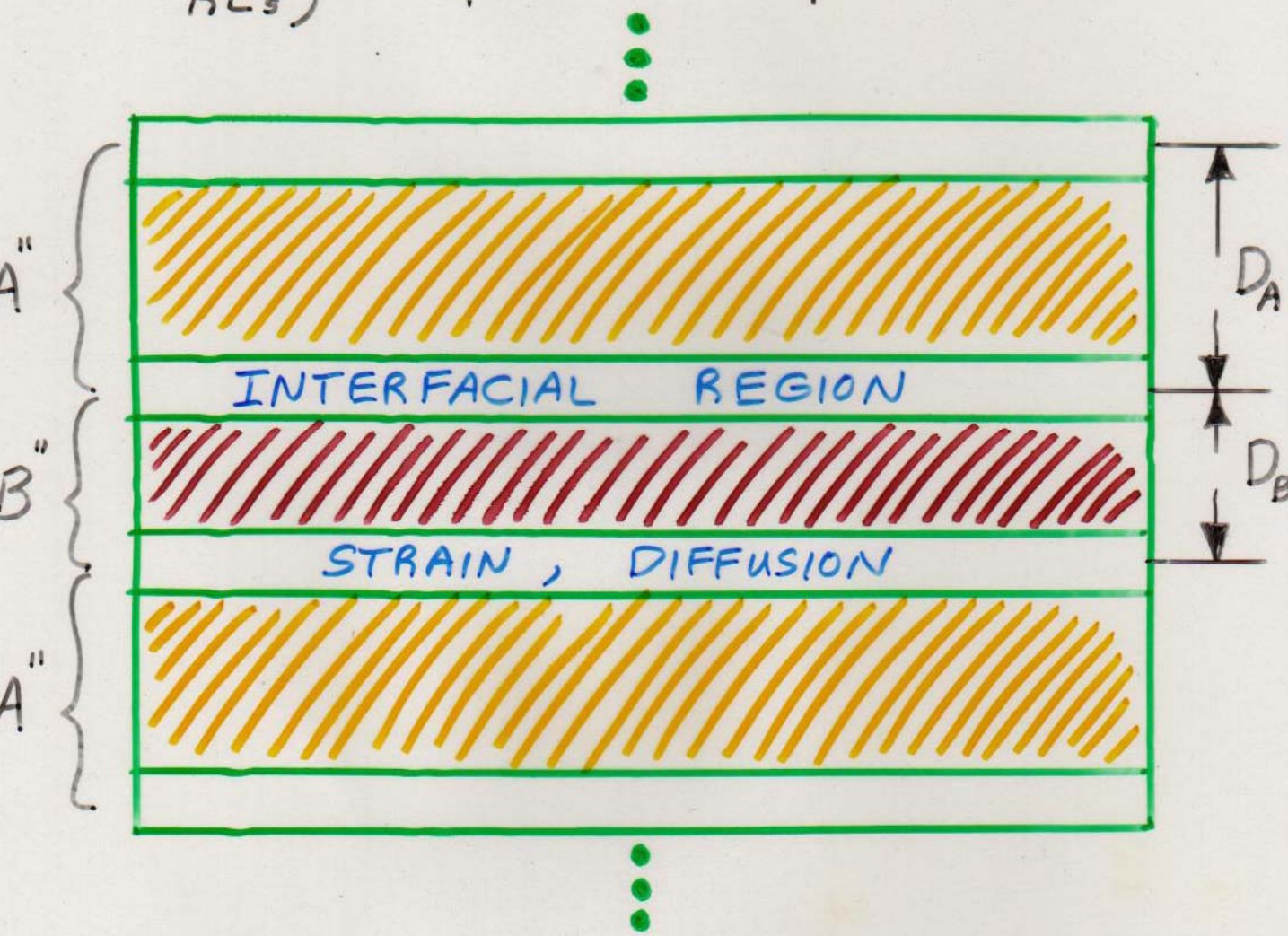

- CRYSTALLOGRAPHIC ORIENTATION
- FINITE SIZE, REDUCED DIMENSIONALITY

Reversible Tuning of the Magnetic Exchange Coupling in Fe/V (001) Superlattices Using Hydrogen

B. Hjörvarsson,[1] J. A. Dura,[2] P. Isberg,[1] T. Watanabe,[2] T. J. Udovic,[2] G. Andersson,[1] and C. F. Majkrzak[2]
[1]*Department of Physics, Uppsala University, Box 530, S-751 21 Uppsala, Sweden*
[2]*National Institute of Standards and Technology, Gaithersburg, Maryland 20899-0001*
(Received 19 February 1997)

The interlayer ordering between ferromagnetic Fe layers in Fe/V (001) superlattices is switched from initially parallel to antiparallel, as well as antiparallel to parallel, upon introducing hydrogen to the V layers. This process is reversible upon removal of the hydrogen. The results unambiguously prove that the major cause of the interlayer coupling transitions is not the hydrogen-induced changes of the thickness of the V layers, but most likely the distortion of the Fermi surface in the V layers. [S0031-9007(97)03652-1]

PACS numbers: 75.70.Cn, 61.12.–q, 68.55.Ln, 75.50.Bb

Magnetic Structure of Cr in Exchange Coupled Fe/Cr(001) Superlattices

A. Schreyer,[1] C. F. Majkrzak,[2] Th. Zeidler,[1] T. Schmitte,[1] P. Bödeker,[1] K. Theis-Bröhl,[1] A. Abromeit,[1] J. A. Dura,[2] and T. Watanabe[2]
[1]*Experimentalphysik (Festkörperphysik), Ruhr-Universität Bochum, 44780 Bochum, Germany*
[2]*National Institute of Standards and Technology, Gaithersburg, Maryland 20899*
(Received 20 February 1997)

We demonstrate how the noncollinear exchange coupling between the Fe layers in Fe/Cr(001) superlattices is caused by a frustrated spiral modulation of the Cr moments not observed in bulk. The noncollinear coupling vanishes above the Néel temperature of this commensurate antiferromagnetic Cr order. This clarifies the essential contribution of Cr ordering to the coupling in the regime of smallest thicknesses where no incommensurate Cr spin density wave can form. For larger Cr thicknesses we observe a predicted incommensurate to commensurate transition with temperature. [S0031-9007(97)04817-5]

PACS numbers: 75.70.Cn, 75.25.+z, 75.30.Fv

Observation of Antiparallel Magnetic Order in Weakly Coupled Co/Cu Multilayers

J. A. Borchers, J. A. Dura, J. Unguris, D. Tulchinsky, M. H. Kelley, and C. F. Majkrzak
National Institute of Standards and Technology, Gaithersburg, Maryland 20899

S. Y. Hsu, R. Loloee, W. P. Pratt, Jr., and J. Bass
Department of Physics and Astronomy, Michigan State University, East Lansing, Michigan 48824
(Received 16 December 1998)

Polarized neutron reflectivity and scanning electron microscopy with polarization analysis are combined to determine the magnetic structure of Co(6 nm)/Cu(6 nm) multilayers. These data resolve a controversy regarding the low-field state of giant-magnetoresistive (GMR) multilayers with weak coupling. As-prepared samples show a strong antiparallel correlation of in-plane ferromagnetic Co domains across the Cu. At the coercive field, the Co domains are uncorrelated. This irreversible transition explains the decrease in magnetoresistance from the as-prepared to the coercive state. For both states, the Co moments reside in domains with in-plane sizes of $\approx 0.5-1.5\ \mu$m. [S0031-9007(99)08797-9]

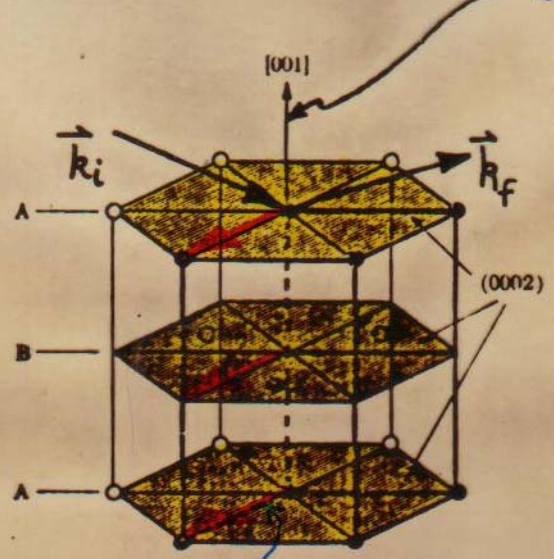

N_{Gd}

μ_{Gd}

J. KWO et al
AT&T

λ_{SL}

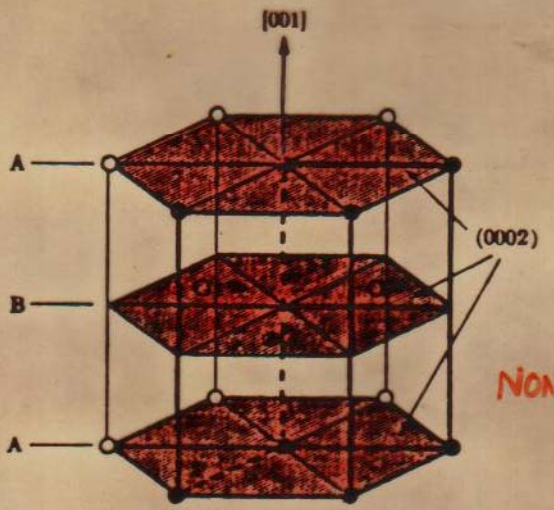

N_Y

NON MAGNETIC

HEXAGONAL CLOSE-PACKED

$[Gd_{N_{Gd}} - Y_{N_Y}]_M$

SEED LAYER Y(002)
BUFFER LAYER Nb (110)
SUBSTRATE Al_2O_3 $(11\bar{2}0)$

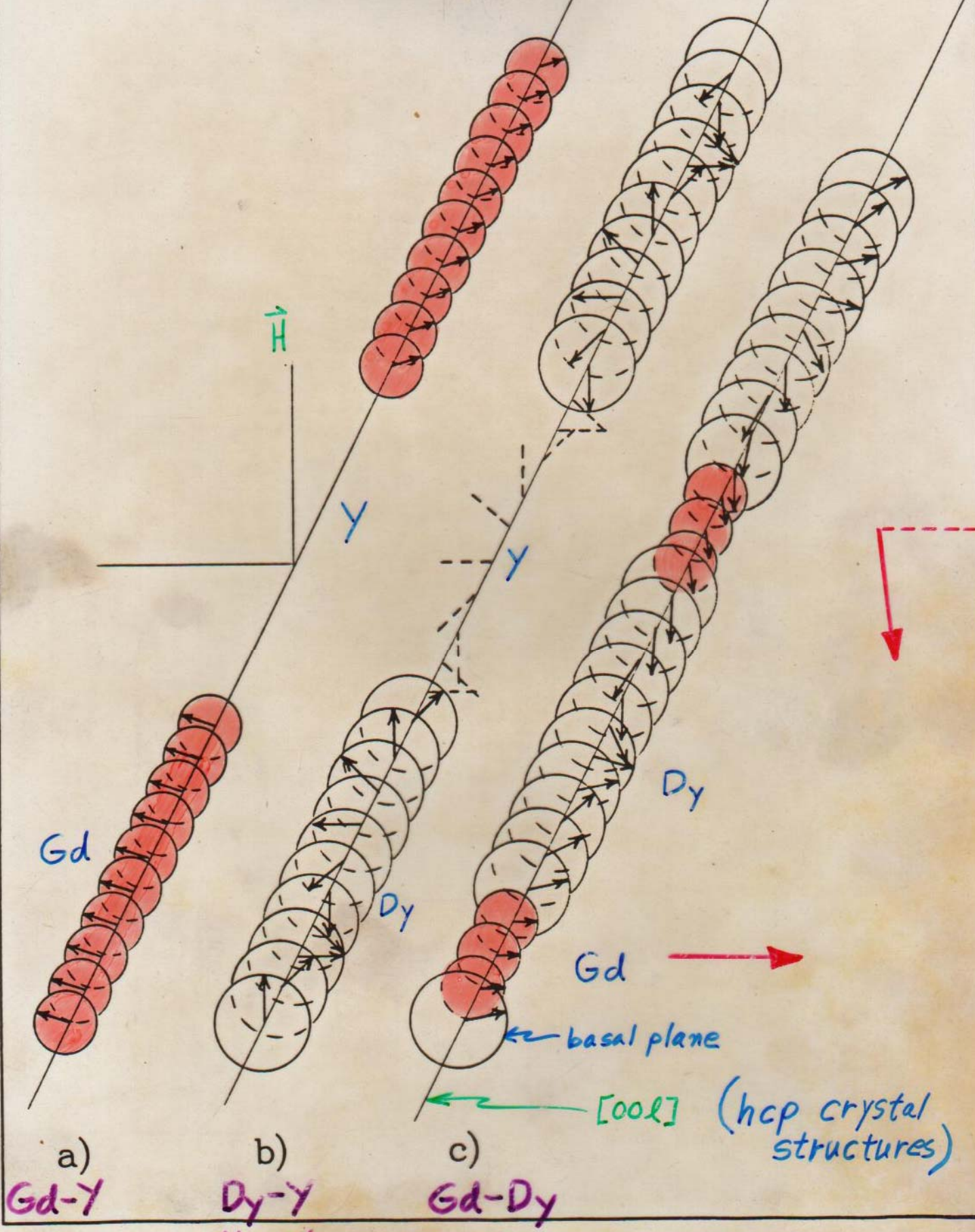
H
Y
Y
Gd
Dy
Dy
Gd
basal plane
[00ℓ]
(hcp crystal structures)
a)
Gd-Y
b)
Dy-Y
Ho-Y
c)
Gd-Dy

FIG. 6

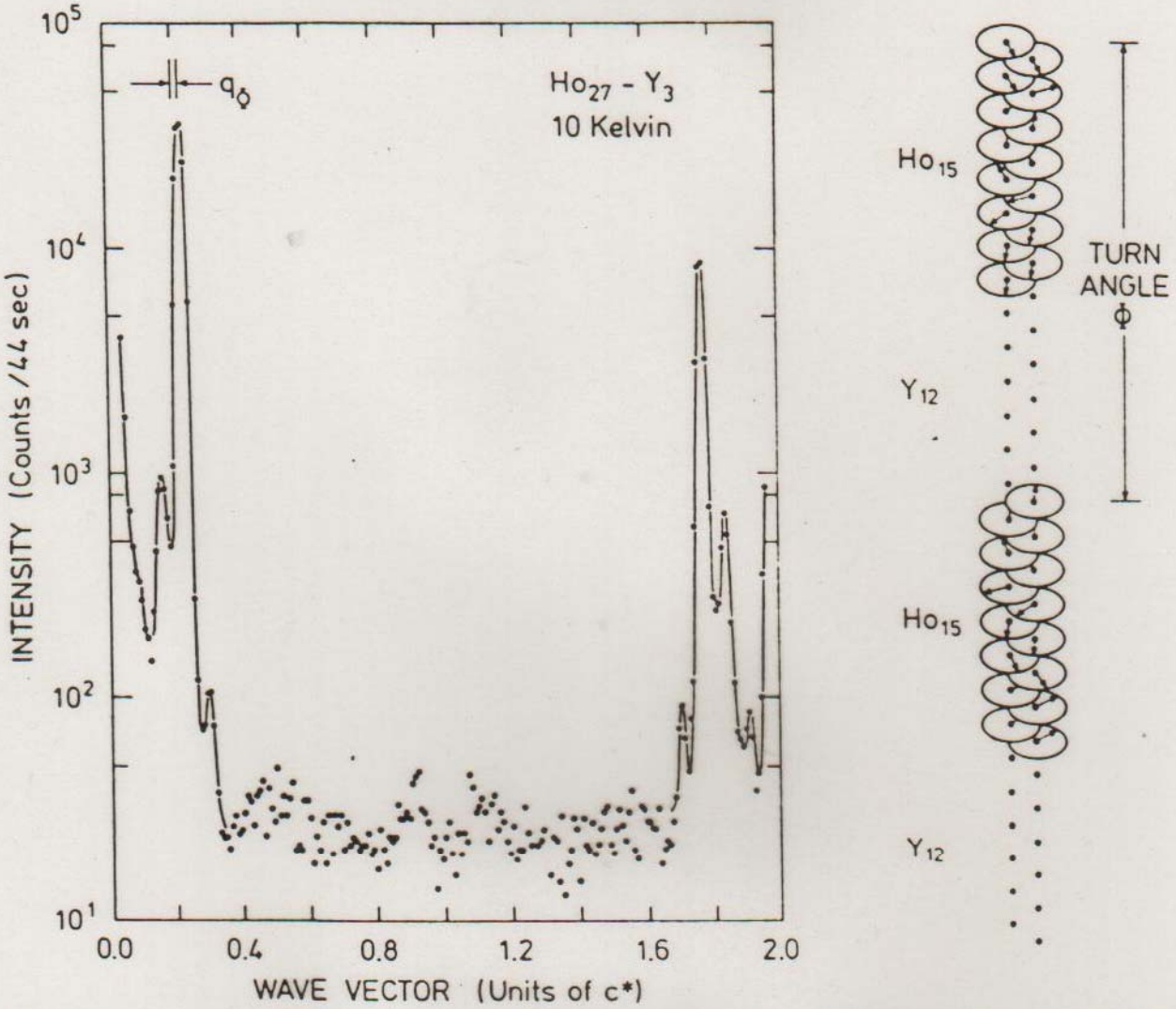

Figure 48. Neutron diffraction pattern obtained from the Ho_{27}–Y_3 superlattice at 10 K. The features of the diffraction pattern are as in figure 8 showing long-range magnetic order. On the right of the figure is shown a schematic drawing of a superlattice explaining the phase advance Φ. The data were taken at Brookhaven on the H9 instrument at the cold source at the HFBR. (After Bohr *et al.* 1989.)

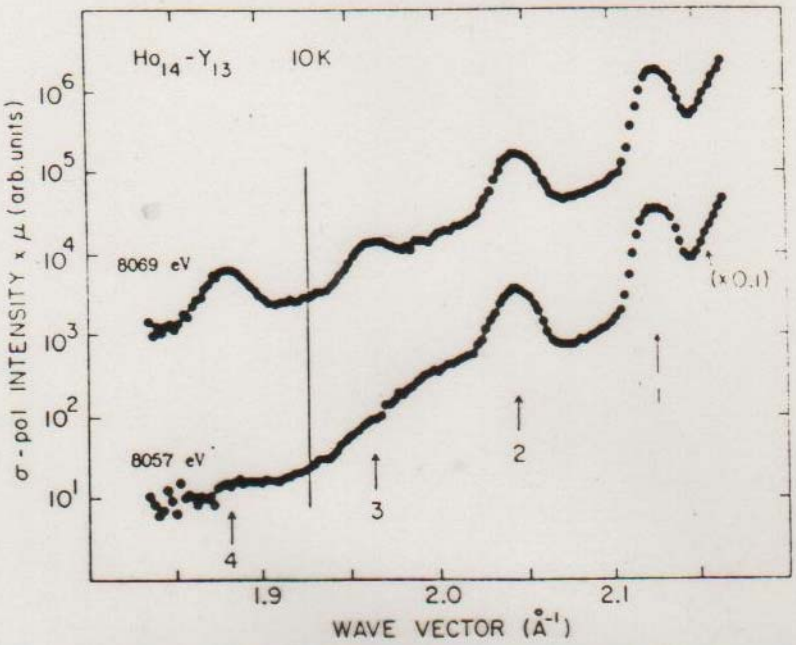

σ → σ channel

$\sigma_{pol.}$ ⇒ linear polarization vec ⊥ diffraction plane

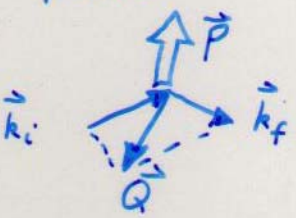

Figure 50. Sigma-polarized X-ray diffraction below the (002) reflection of the Ho_{14}–Y_{13} superlattice at 10 K for two different incident X-ray energies. Arrows indicate the positions of the 1st to 4th harmonics of the charge scattering. The solid line indicates the position of the central peak of the magnetic scattering (Gibbs *et al.* 1989, unpublished).

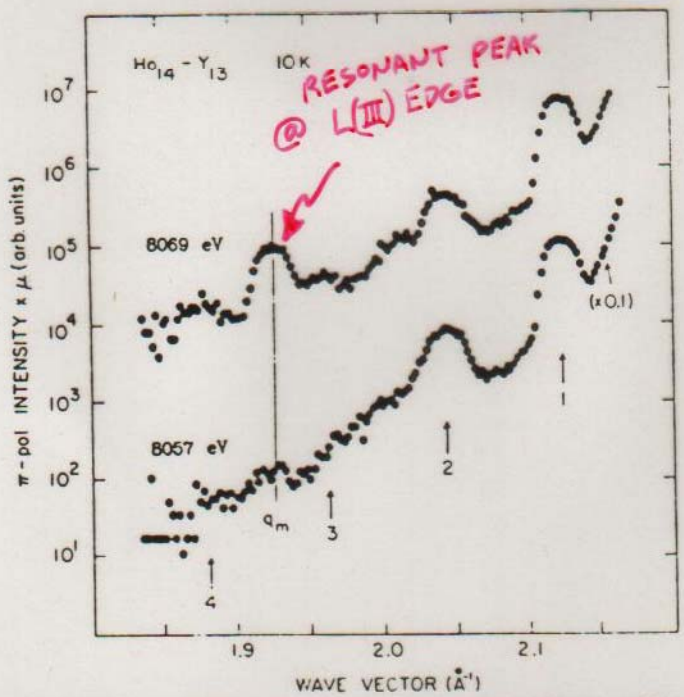

σ → π channel

$\pi_{pol.}$ ⇒ linear polarization vector ∥ diffraction plane

Figure 51. π-polarized X-ray diffraction pattern below the (002) reflection of Ho_{14}–Y_{13} at 10 K for two different incident X-ray energies. As in figure 50, the arrows indicate charge peaks and the solid line the central position of the magnetic scattering (Gibbs *et al.* 1989, unpublished).

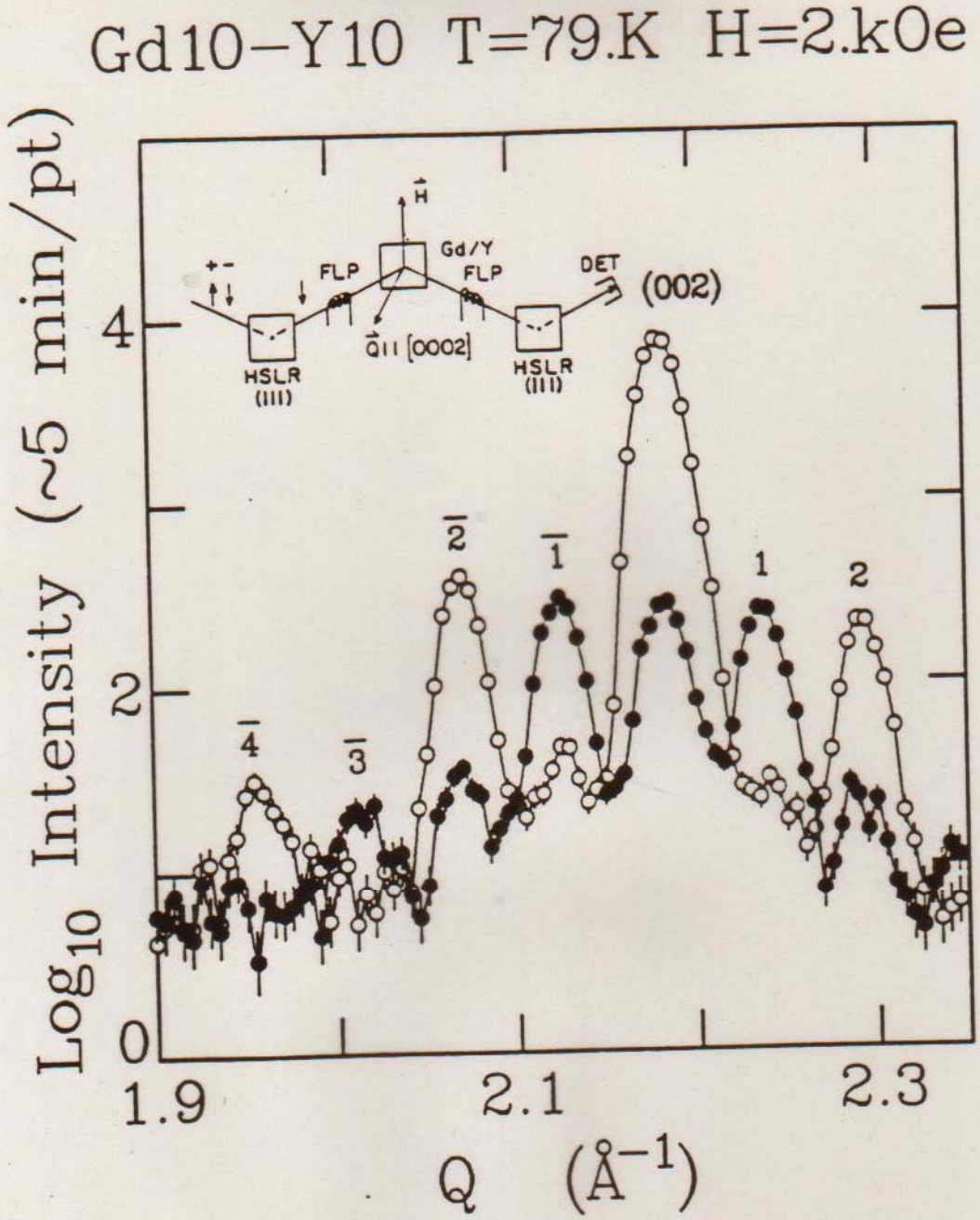

Fig. 7–1

Figure 7-1. NSF (open circles) and SF (filled circles) scattering from a [Gd_{10} - Y_{10}] superlattice as described in the text. The data have not been corrected for instrumental polarizing and flipping efficiencies (the SF scattering at the (002) position is predominantly, if not entirely, instrumental in origin). The SF scattering which appears at values of Q corresponding to a doubling of the chemical bilayer spacing (odd-numbered satellites) is consistent with an antiferromagnetic alignment (for an applied field approaching zero) of neighboring ferromagnetic Gd layers as depicted schematically in Figure 7-2. (After Majkrzak et al. (1986)).

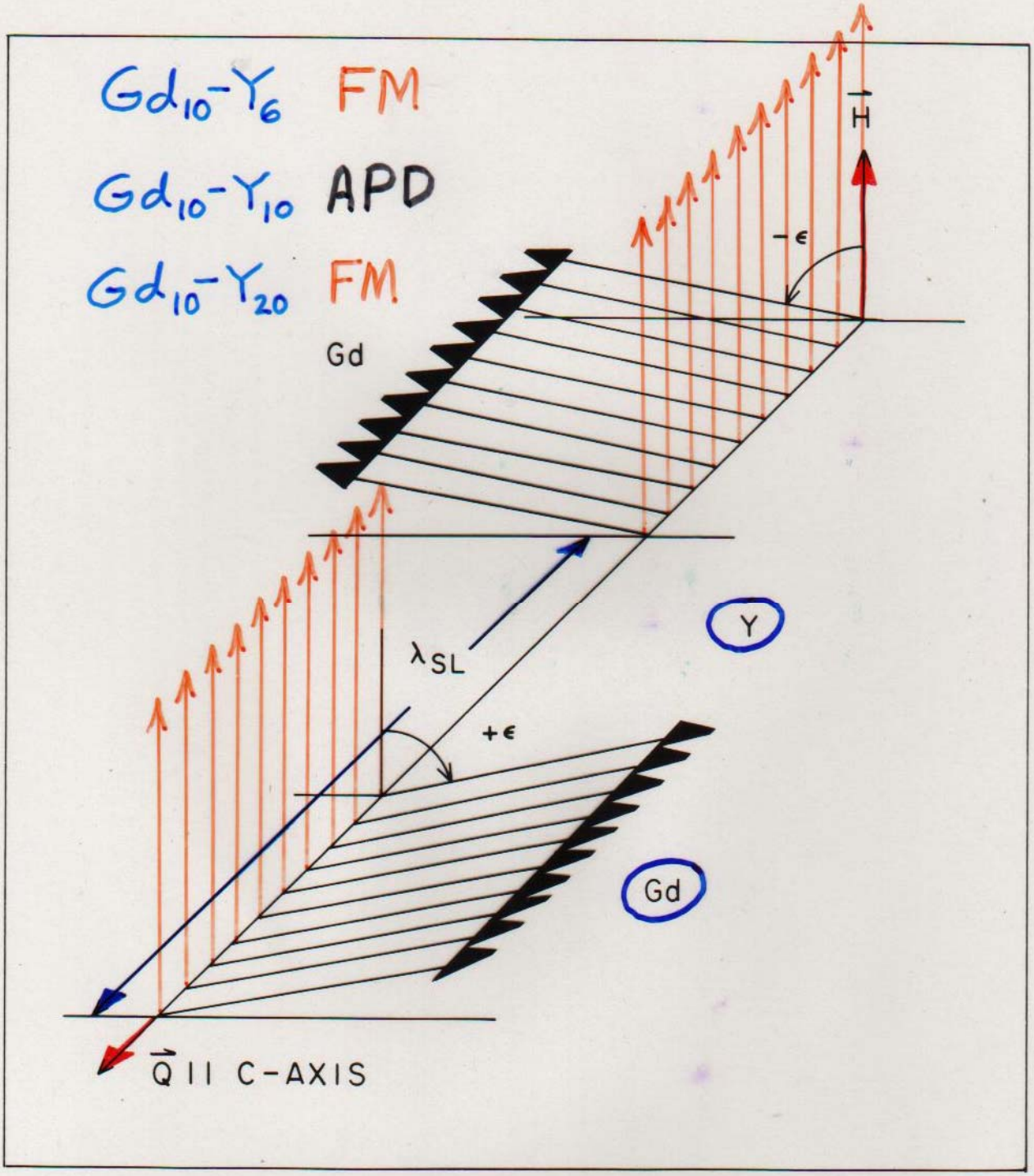
Gd_{10}-Y_6 FM
Gd_{10}-Y_{10} APD
Gd_{10}-Y_{20} FM
Gd
$\vec{H}$
$-\epsilon$
λ_{SL}
$+\epsilon$
Y
Gd
$\vec{Q}$ II C-AXIS

n-diffr. meas.

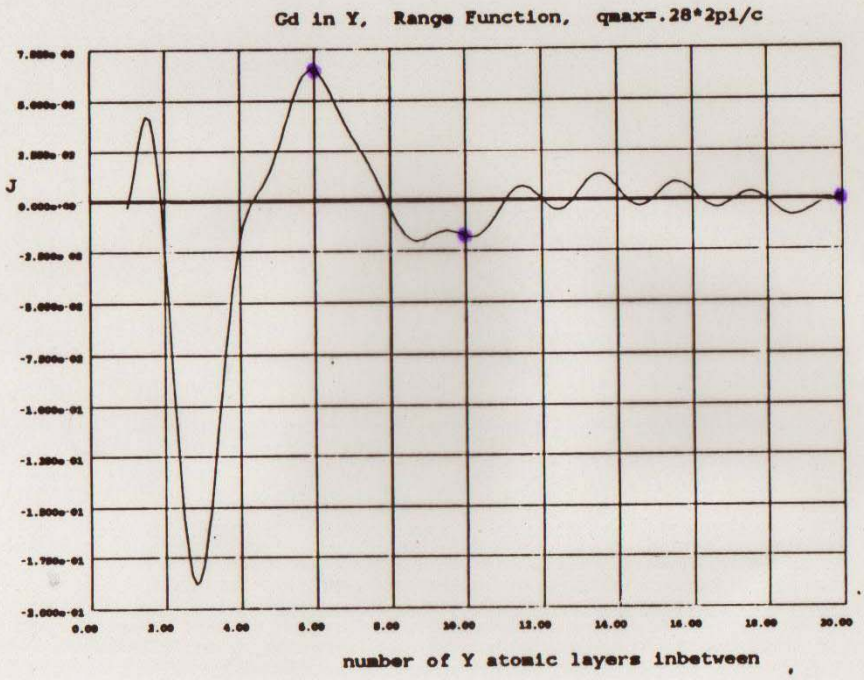
Gd in Y, Range Function, qmax=.28*2pi/c
J
0.00
2.00
4.00
6.00
8.00
10.00
12.00
14.00
16.00
18.00
20.00
number of Y atomic layers inbetween

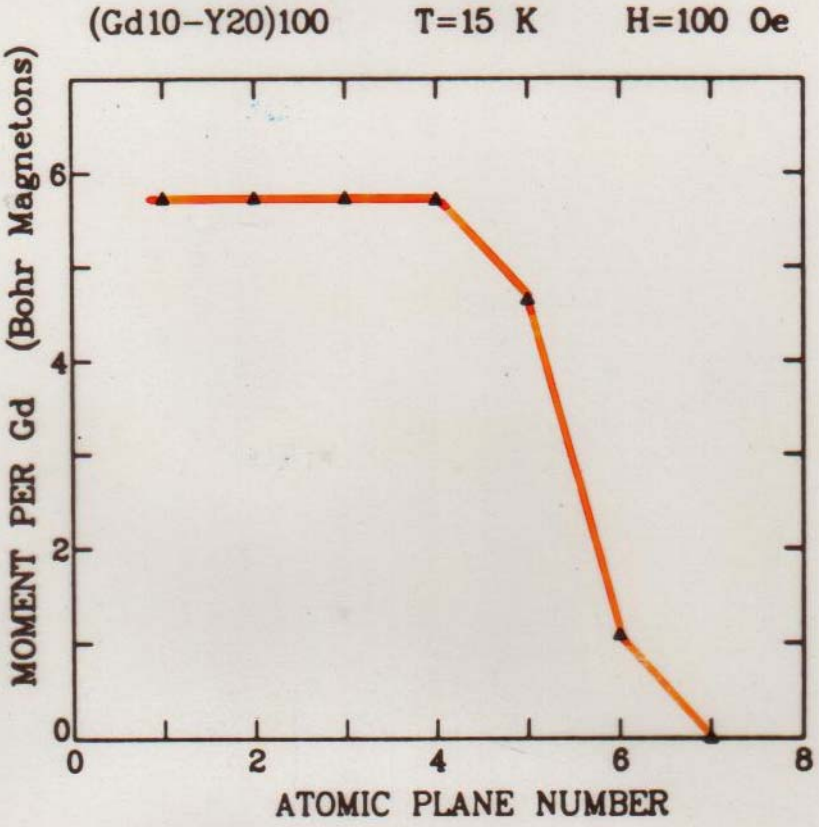

Fig. 7 Magnetization profile across a Gd layer in a Gd-Y superlattice deduced from polarized neutron reflection data as described in the text. Atomic plane #1 is at the center of the layer whereas the center of the interfacial region is between planes 5 and 6 (from Ref. 16).

MAJKRZAK, CABLE, KWO, HONG, McWHAN, YAFET, WASZCZAK, GRIMM, & VETTIER, J. APPL. PHYS. 61, 4055 (1987).

→ USING STRAIN AND COMPOSITION MODULATION PROFILES OBTAINED FROM X-RAY DIFFRACTION MEASUREMENTS : VETTIER, McWHAN, GYORGY, KWO, BUNTSCHUH, & BATTERMAN, PHYS. REV. LETT. 56, 757 (1986).

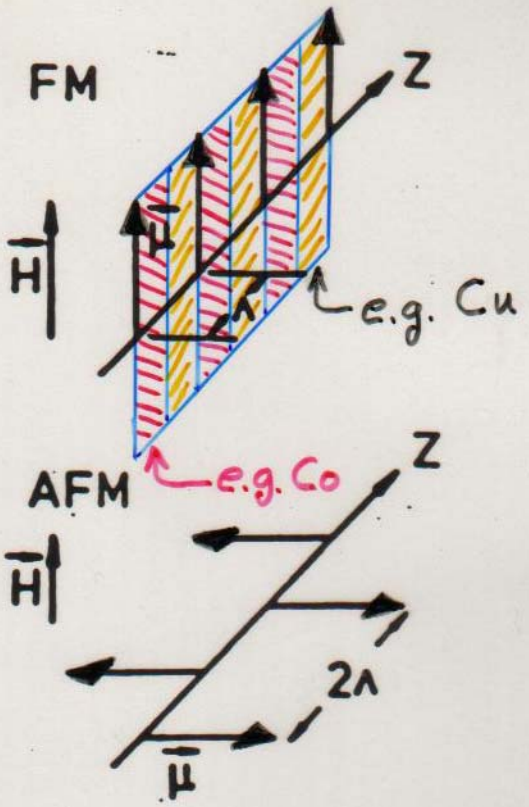

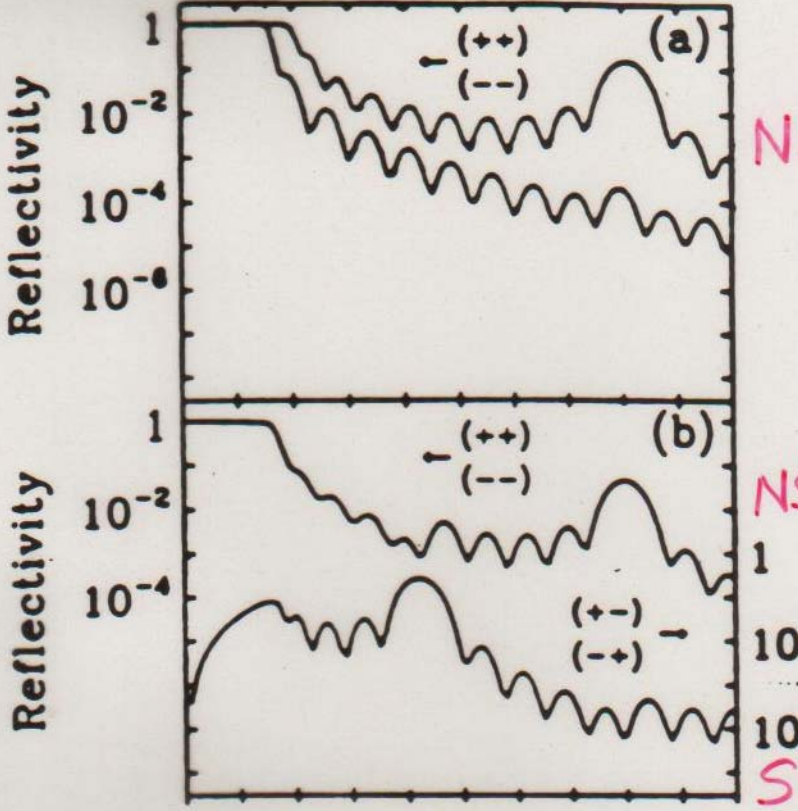

"GIANT" MAGNETORESISTANCE (GMR) EFFECT:

FM ⇒ LOW RESISTANCE

AFM ⇒ HIGH RESISTANCE

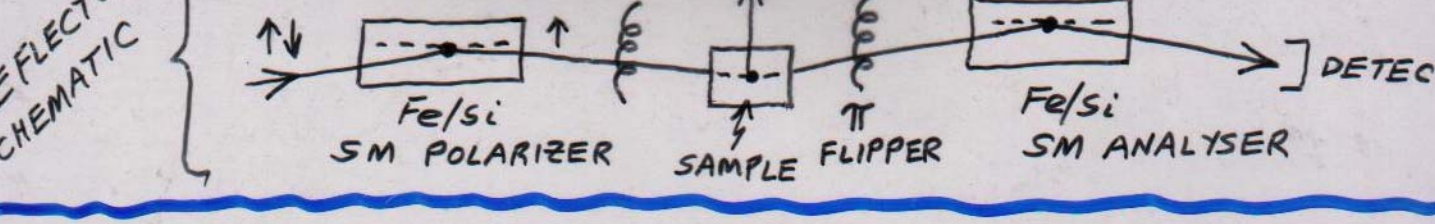

POLARIZED NEUTRON REFLECTIVITY MEASUREMENT ON A Co/Cu SUPERLATTICE PERFORMED AT NIST

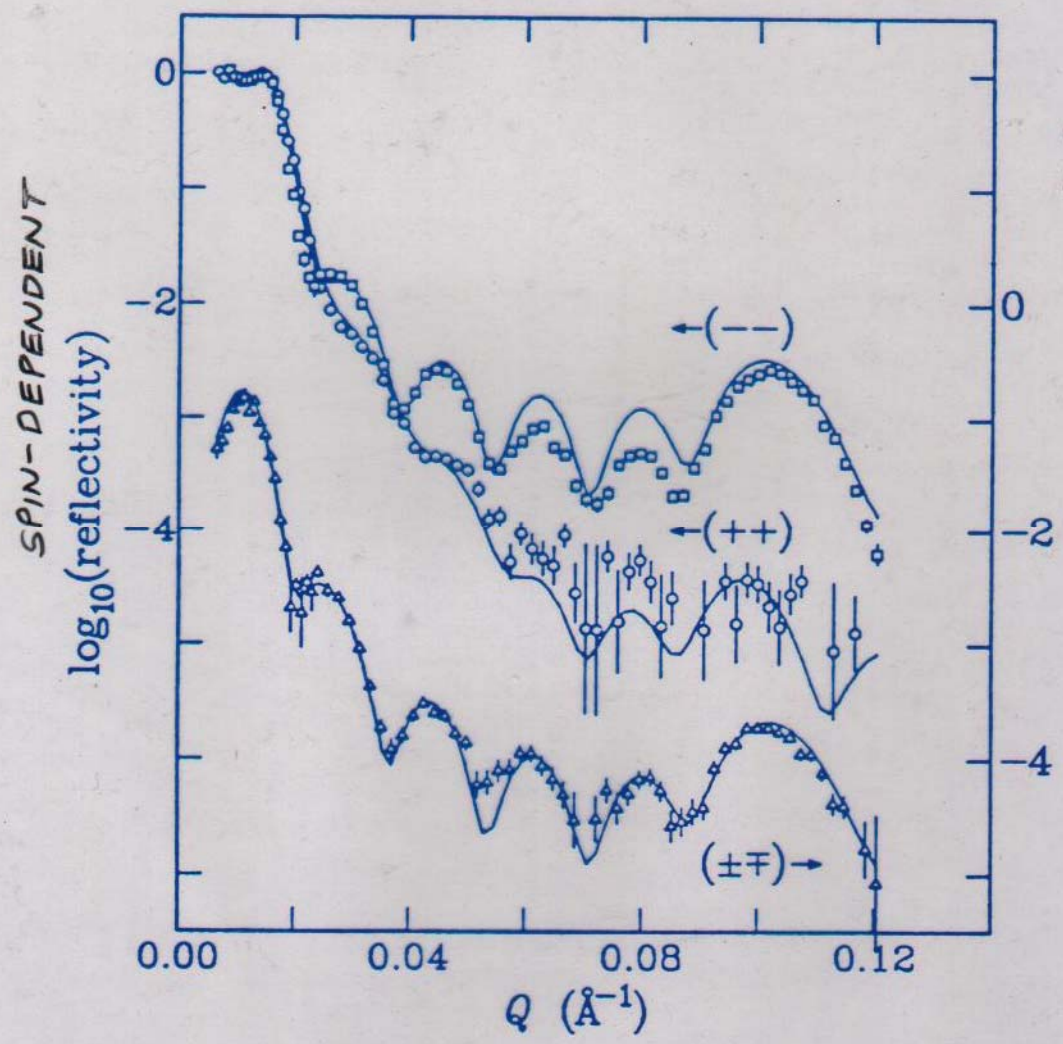

A. SCHREYE
J. ANKNER
C. MAJKRZA
H. ZABEL
et al.

SAMPLE VOLUME < ONE MILLIONTH OF CUBIC CENTIMETER

PROFILES AS A FUNCTION OF DEPTH INTO FILM SURFACE AS RECONSTRUCTED FROM DYNAMICAL FIT OF REFLECTIVITY DATA OF PRECEDING FIGURE

Co/Cu SUPERLATTICE

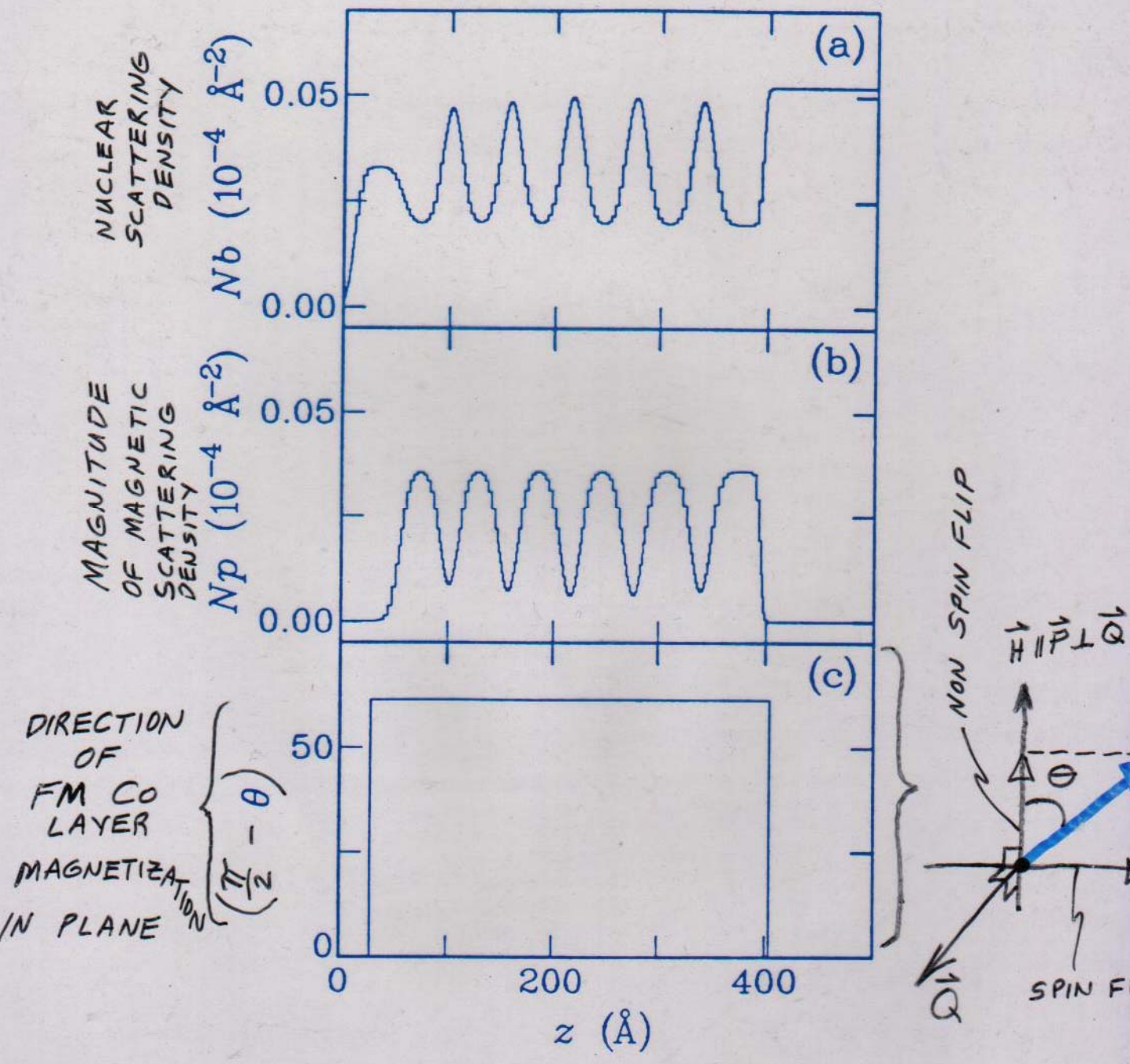

X-RAY RESONANT MAGNETIC SCATTERING

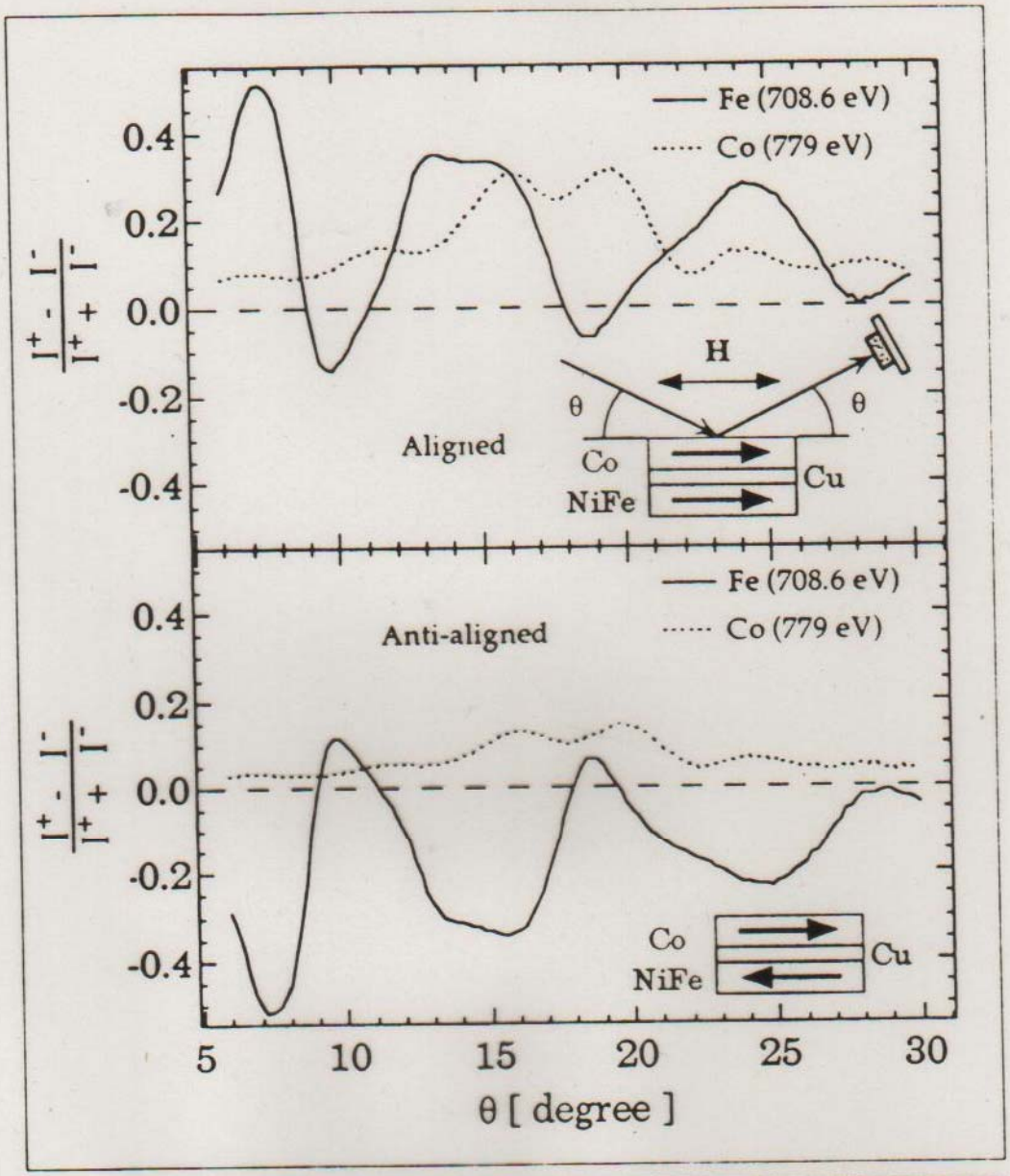

Figure 9. Top Panel: XRMS asymmetry curve for Fe (solid) and Co (dashed) at the respective L3 resonance energies in aligned state (pt. A-A') as a function of scattering angle. Inset scattering geometry. Bottom Panel: XRMS asymmetry for anti-aligned state (pt. B-B').

(Y. IDZERDA et al.)

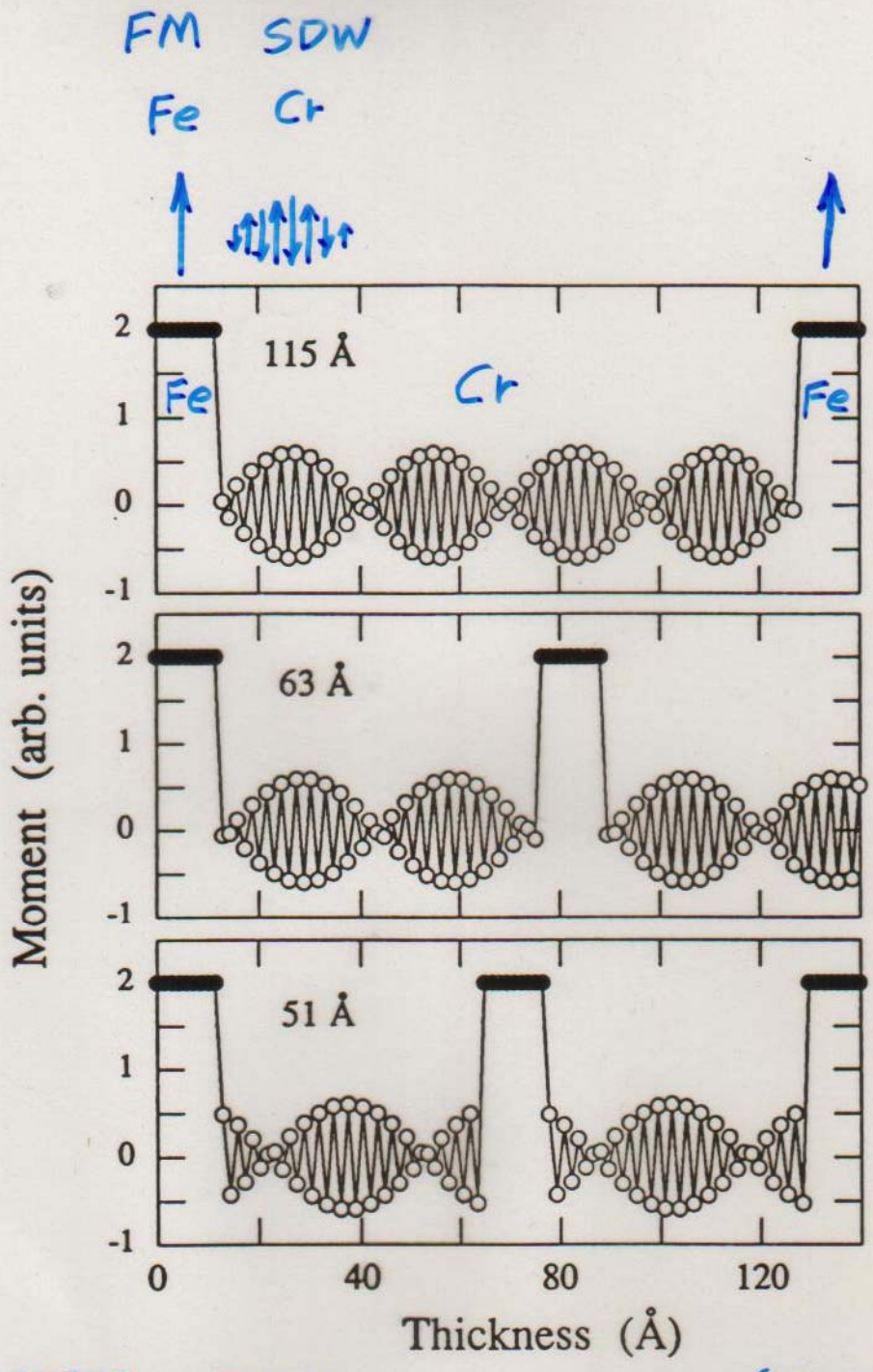

Fe/Cr SUPERLATTICES (GMR)

FULLERTON, BADER, & ROBERTSON

Figure 3

NON COLLINEAR Fe/Cr (001)

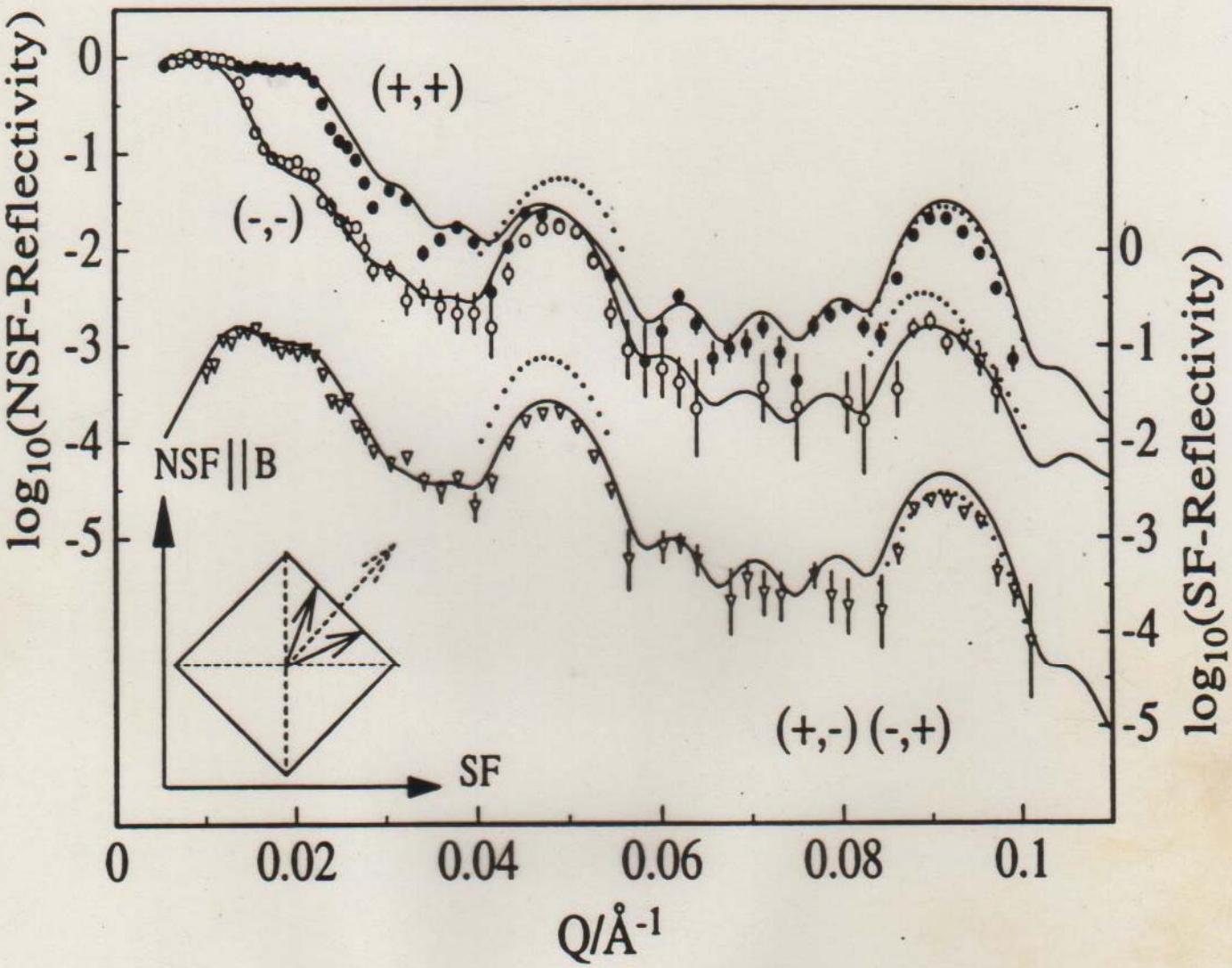

..... 90° ∡

—— 50° ∡

$$E = -J_1 \frac{\vec{M}_1 \cdot \vec{M}_2}{|\vec{M}_1||\vec{M}_2|} - J_2 \left(\frac{\vec{M}_1 \cdot \vec{M}_2}{|\vec{M}_1||\vec{M}_2|} \right)^2$$

EXCHANGE COUPLING

BILINEAR

BIQUADRATIC

A. Schreyer etal.

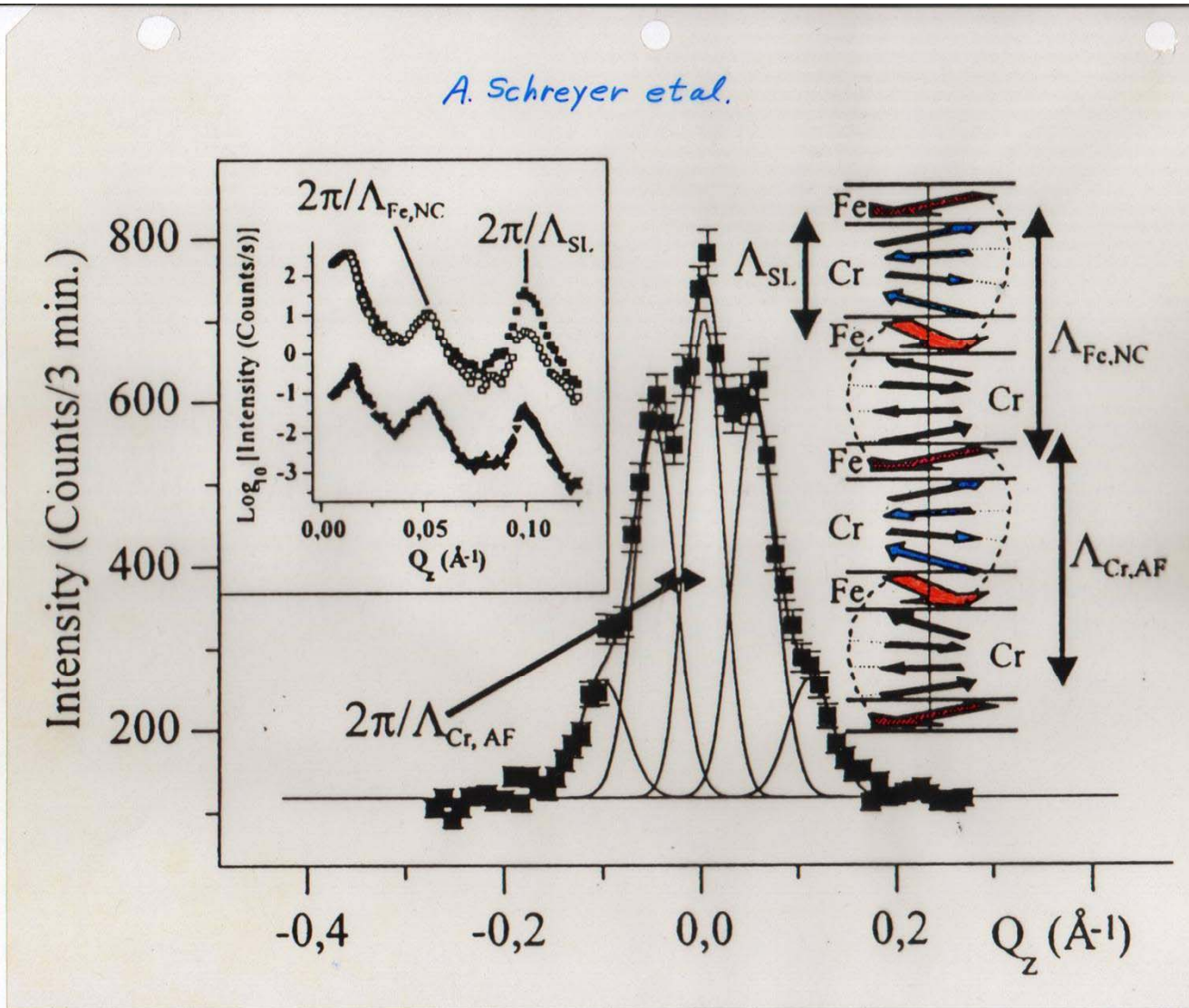

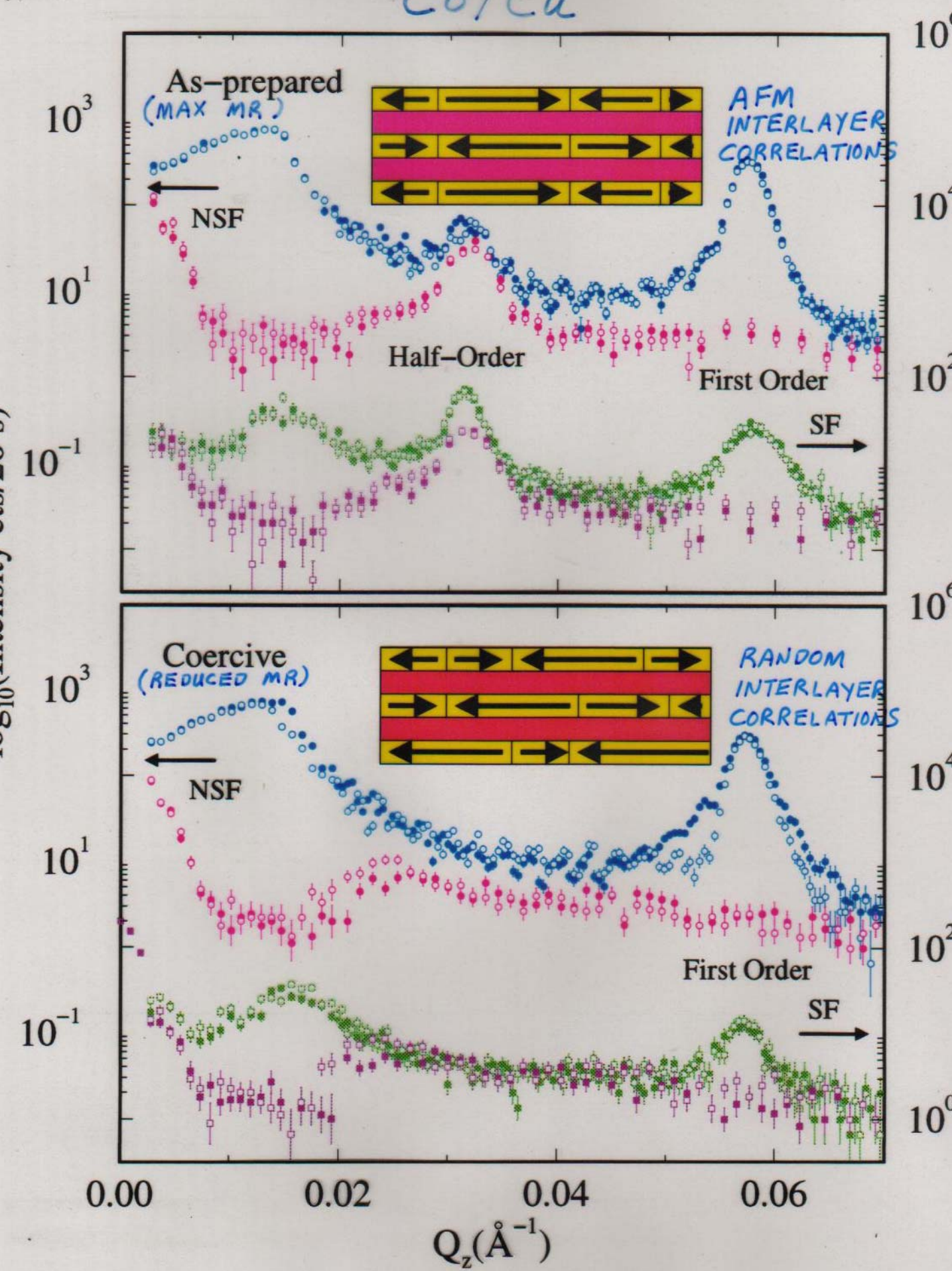
Co/Cu
As–prepared
(MAX MR)
AFM
INTERLAYER
CORRELATIONS
NSF
Half–Order
First Order
SF
Coercive
(REDUCED MR)
RANDOM
INTERLAYER
CORRELATIONS
NSF
First Order
SF
10^3
10^1
10^{-1}
0.00
0.02
0.04
0.06
$Q_z(\text{Å}^{-1})$

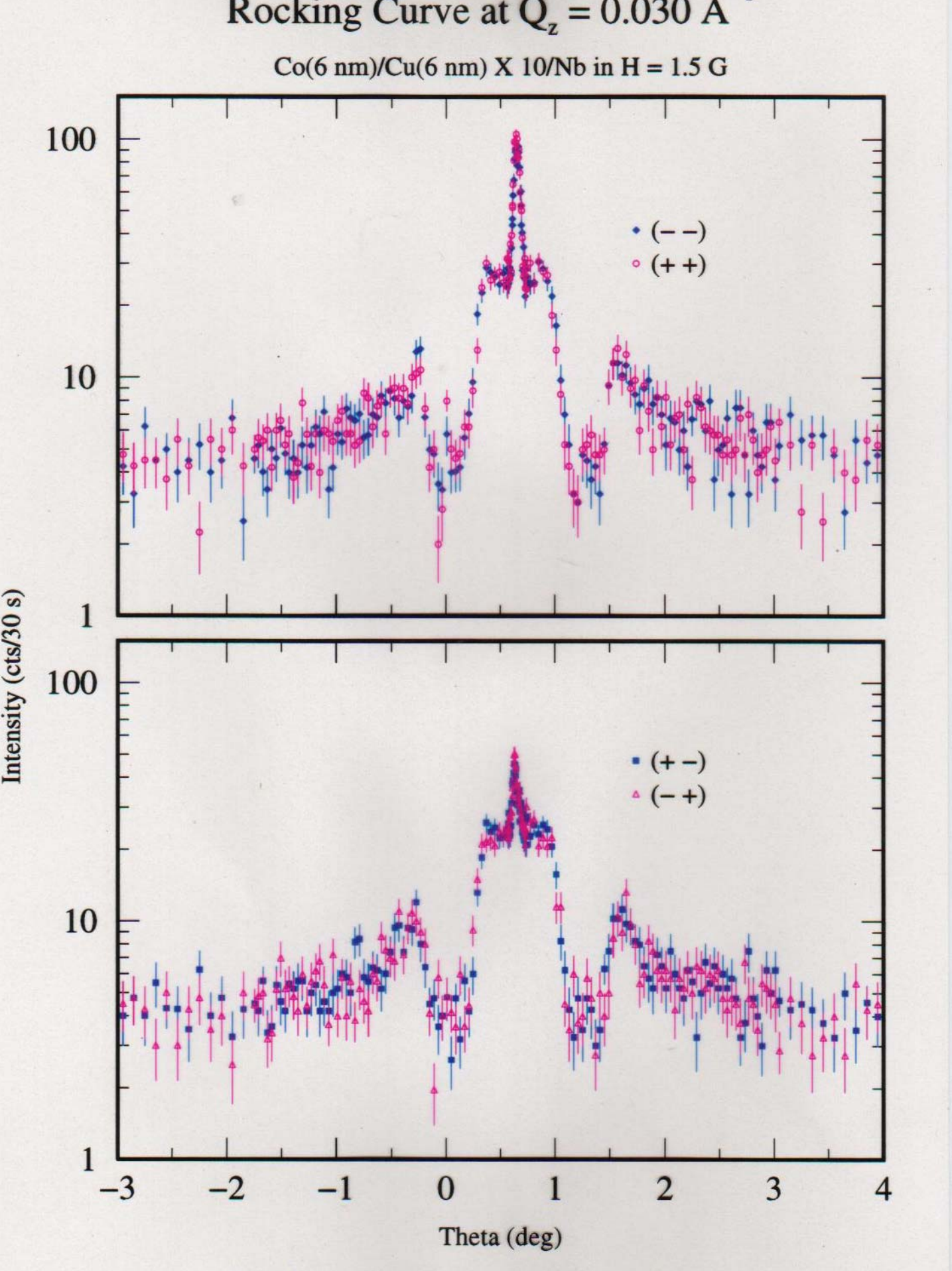
Rocking Curve at Q_z = 0.030 Å^{-1}
Co(6 nm)/Cu(6 nm) X 10/Nb in H = 1.5 G
100
10
1
(− −)
(+ +)
100
10
1
(+ −)
(− +)
Intensity (cts/30 s)
−3
−2
−1
0
1
2
3
4
Theta (deg)

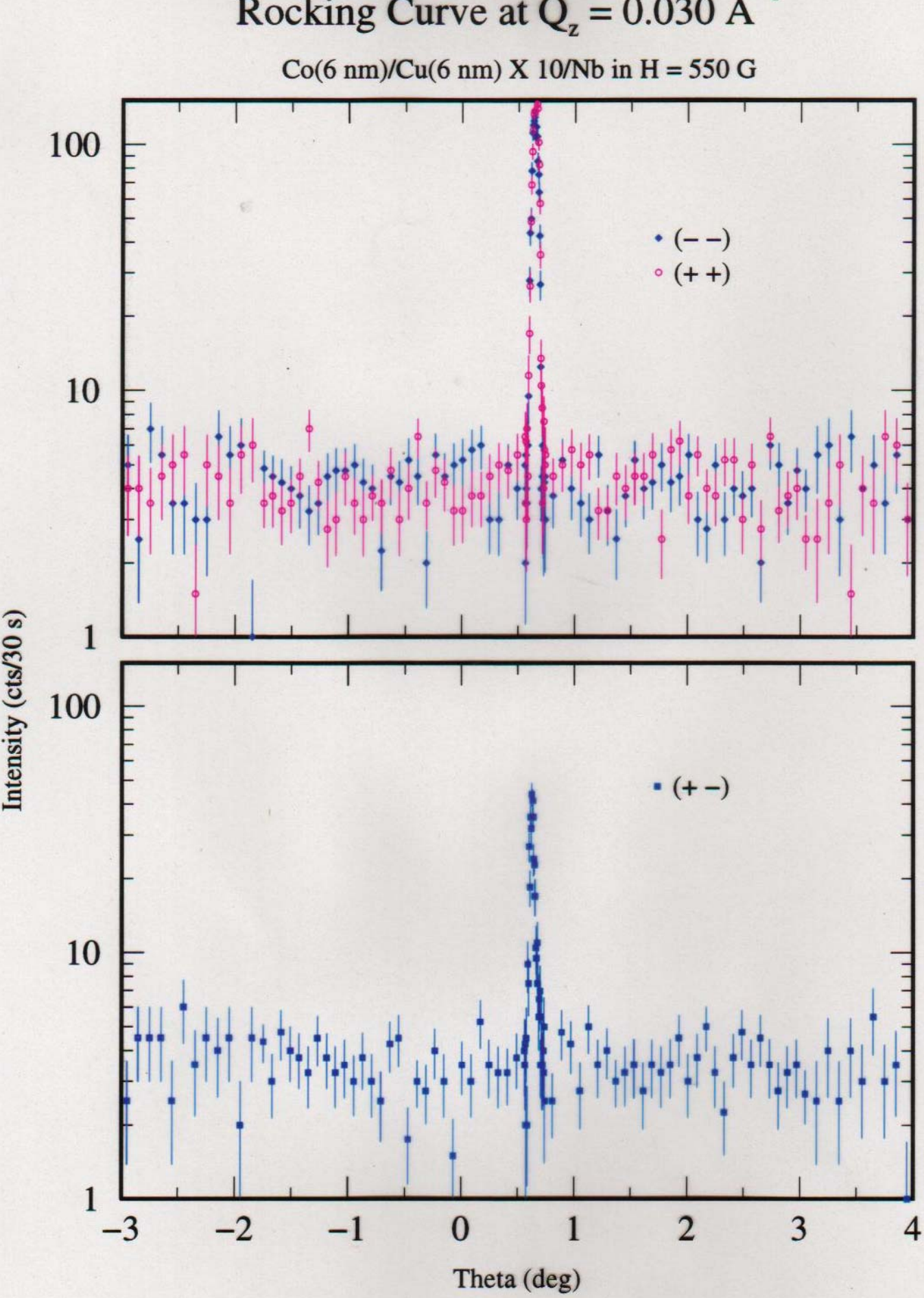
Rocking Curve at Q_z = 0.030 Å^{-1}
Co(6 nm)/Cu(6 nm) X 10/Nb in H = 550 G
100
10
1
(– –)
(+ +)
100
10
1
(+ –)
Intensity (cts/30 s)
–3
–2
–1
0
1
2
3
4
Theta (deg)

Magnetic Semiconductor Superlattices

Currently a great deal of attention is being focused on spintronics, a new area of solid-state electronics. In spintronics not only the electric current but also its spin state is controlled. Spin valves and spin injectors are the first practical applications of spintronics. Further progress in developing new devices hinges critically on the availability of suitable materials. Such materials need to be ?good? semiconductors, easy to integrate in typical integrated circuits, and their electronic properties should exhibit strong sensitivity to the carrier?s spin, ferromagnetism being an especially desirable property.

EuS is one of the very few natural ferromagnetic (F M) semiconductors. Since it becomes F M at a low temperature (T_c = 16.6 K) it is an unlikely choice for applications. However, studying the properties of heterostructures made on its base may give an important insight into fundamental processes taking place in all classes of materials under consideration.

GaMnAs is a man-made F M semiconductor. It is an example of a diluted magnetic semiconductor (D M S) in which a fraction of nonmagnetic cations (Ga) is substituted with magnetic ions (Mn). Such a material can readily be incorporated into modern GaAs-based semiconductor devices. Its T_c is still below room temperature, but this limitation may be lifted in other materials of this class (Refer to Reference 1).

Interlayer exchange coupling (I E C) in superlattices (S L), composed of ferromagnetic and nonmagnetic layers, is a crucial element of all spin-valve type devices that utilize the giant magnetoresistance effect. In metallic S L's currently being used, conduction electrons transfer the interlayer interactions through nonmagnetic spacers (Refer to Reference 2). Here we address the question whether I E C phenomena are possible in all-semiconductor superlattices, like EuS/PbS and GaMnAs/GaAs, where the carrier concentrations are many orders of magnitude lower than in metals.

The nonmagnetic spacer in EuS/PbS S L's is a narrow gap semiconductor with electron concentration of the order of 10^{17} cm^{-3} to 10^{18} cm^{-3}. For thin PbS layers ($d_{PbS} < 70$ Å) neutron reflectivity spectra, shown in Figure 1, have revealed a pronounced maximum of magnetic origin at the position corresponding to the doubled structural S L periodicity, thus indicating the existence of antiferromagnetic (A F M) interlayer arrangements (Refer to Reference 3).

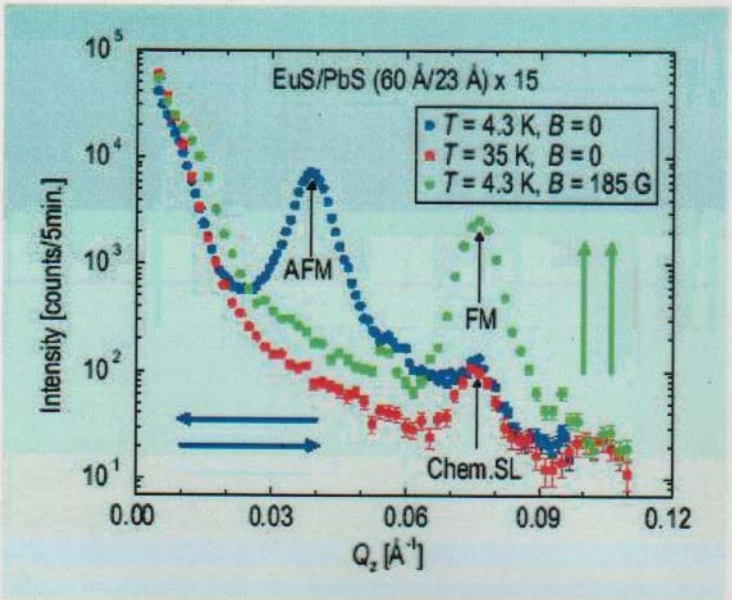

FIGURE 1. Unpolarized neutron reflectivity spectra for EuS/PbS S L with thin (23 Å) PbS spacer. Antiferromagnetic interlayer exchange coupling below T_c and at zero external field is clearly visible (blue curve). Applying a strong enough magnetic field (185 G in this case) parallel to the S L surface forces all the EuS layer?s magnetizations to ferromagnetic configuration (green curve). Above T_c the system is nonmagnetic, the only Bragg peak comes from the chemical S L periodicity.

For much thicker PbS spacers (d_{PbS} > 120 Å) the only magnetic peaks visible in the reflectivity profiles, see example in Figure 2, coincide with the chemical ones, thus leading to the conclusion that the magnetization vectors in adjacent EuS layers are parallel, which indicates F M I E C.

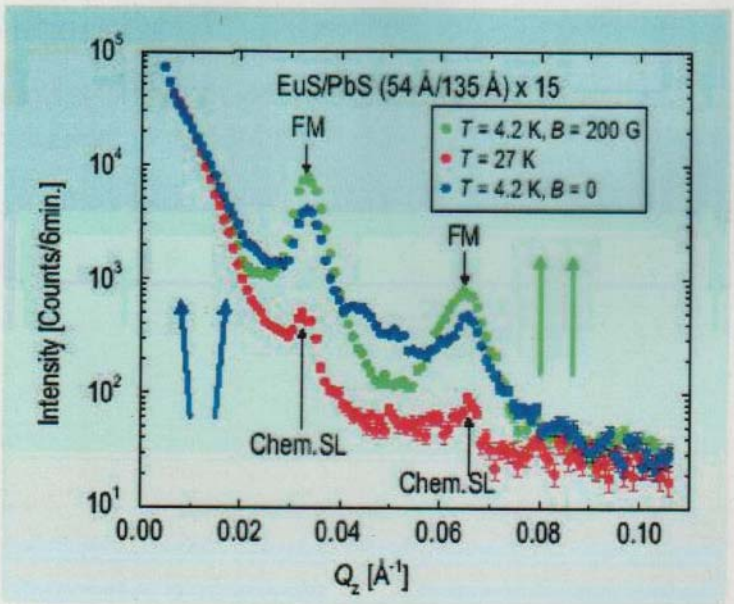

FIGURE 2. The sample with thick (135 Å) PbS layers is almost ferromagnetically coupled. Application of an external magnetic field enhances the F M Bragg peaks and lowers the intensity between them (at the A F M peak position).

In the intermediate PbS thickness range (70 Å < d_{PbS} < 120 Å), both A F M and F M peaks are present. Polarized neutron analysis of these maxima gives evidence that the magnetization vectors of adjacent EuS layers are not colinear. Hence, the I E C found in EuS/PbS S L's has an oscillatory character similar to that occurring in metallic S L's, although the oscillation period is much longer than the one in metallic systems.

In order to confirm that the free carriers, present in the PbS layer in such a small amount, are the cause of the observed oscillatory I E C, a series of analogous measurements have been carried out on EuS/YbSe S L's. The structure and lattice constant of YbSe are the same as those of PbS. In contrast to PbS, YbSe is a semi-insulator with a negligible carrier concentration. Neutron reflectivity profiles have shown no evidence of any interlayer coupling in the all investigated samples. That finding, together with the oscillatory character of coupling in S L's with PbS spacer, strongly points to the leading role of PbS free electrons in providing the necessary I E C mechanism, similar to that discovered in metallic multilayers.

Ferromagnetic ordering in GaMnAs is carrier (holes) induced; the Mn atoms, apart from being the magnetic element in the system, act also as acceptors providing the holes responsible for transferring exchange interactions between them. The details of the magnetic ordering, in particular its range, are still being disputed.

To address the latter issue, polarized neutron reflectometry has been performed on a number of GaMnAs/GaAs superlattices. Figure 3 shows an example of the obtained reflectivity profile in the vicinity of the first S L Bragg peak, for one of the samples. The very presence of the magnetic contribution to the structural S L Bragg peak is a strong confirmation of the F M I E C between consecutive GaMnAs layers. The absence of any spin-flip scattering shows that the sample is in a one-domain state, i.e., the F M ordering in GaMnAs is long range, and the sample is spontaneously saturated. The peak in (--) cross section, and its absence in the (++), is proof that the magnetization is directed oppositely to the external magnetic guide field, hence the long range ordering has formed spontaneously, without the influence of the external field. More details can be found in Reference 4.

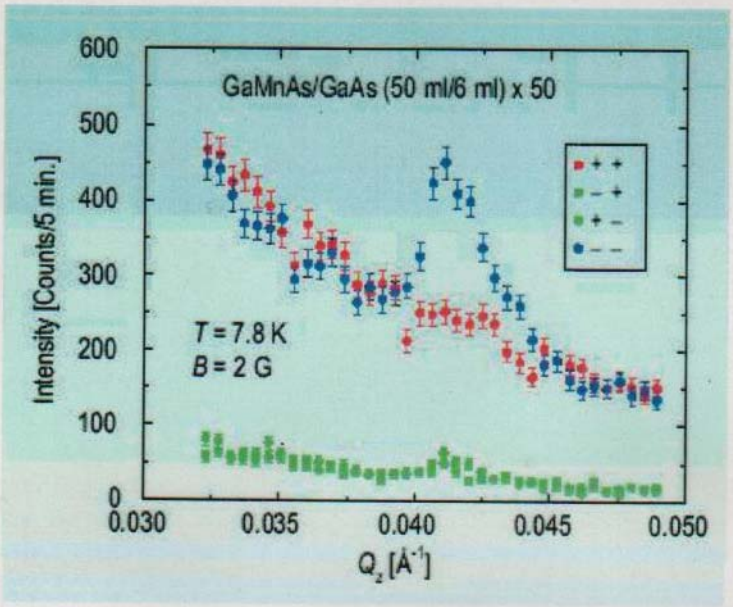

FIGURE 3. Polarized neutron reflectivity spectra for GaMnAs/GaAs superlattice.

References

[1] T. Dietl, H. Ohno, F. Matsukura, J. Cibert, D. Ferrand, Science 287,1018 (2000).

[2] P. Bruno, Phys. Rev. B52, 411 (1995).

[3] H. Kepa, J. Kutner-Pielaszek, J. Blinowski, A. Twardowski, C. F. Majkrzak, T. Story, P. Kacman, R. R. Galazka, K. Ha, H. J. M. Swagten, W. J. M de Jonge, A. Yu. Sipatov, V. Volobuev, T. M. Giebultowicz, Europhys. Lett. 56, 54 (2001).

[4] H. Kepa, J. Kutner-Pielaszek, A. Twardowski, C. F. Majkrzak, J. Sadowski, T. Story, T. M. Giebultowicz, Phys. Rev. B64, 121302 (2001).

Authors

A. Yu. Sipatov, V. Volobuev
Kharkov State Polytechnical University
Kharkov, Ukraine

H. Kepa, J. Kutner-Pielaszek, A. Twardowski
Institute of Experimental Physics
Warsaw University
Warsaw, Poland

T. Story, J. Sadowski
Institute of Physics
Polish Academy of Sciences
Warsaw, Poland

T. M. Giebultowicz
Physics Department
Oregon State University
Corvallis, OR 97331

C. F. Majkrzak
N I S T Center for Neutron Research
National Institute of Standards and Technology
Gaithersburg, MD 20899-8562

Back to Reflectometry Scientific Highlights

Last modified 15-January-2003

T. GIEBULTOWICZ ET AL.

(111) $[(EuTe)_m|(PbTe)_n]_N$ Antiferromagnetic Superlattices:

Magnetically Correlated multilayers vs. Uncorrelated ones

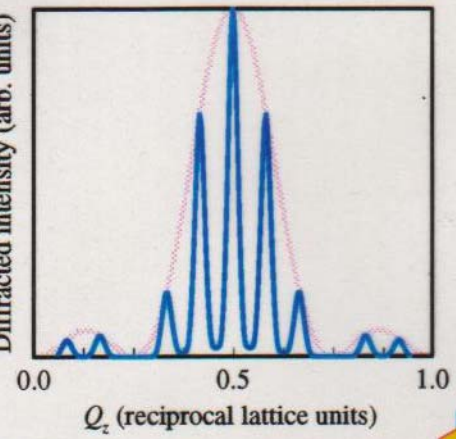

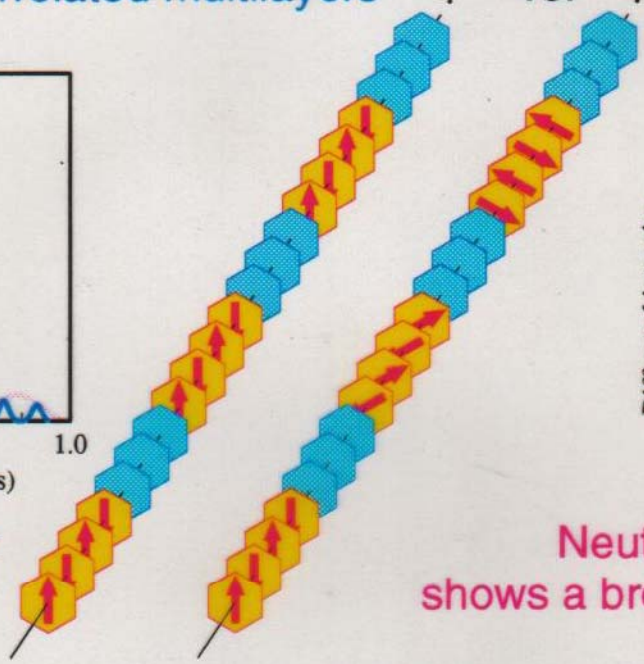

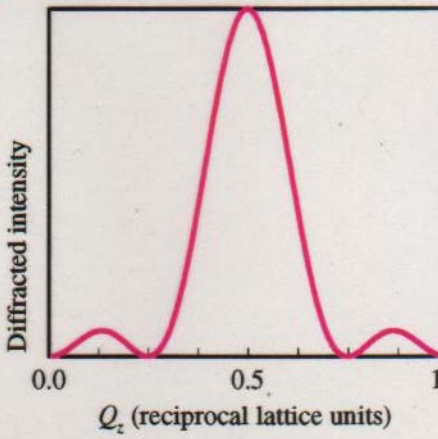

Diffraction pattern: many narrow fringes

Neutron diffraction pattern shows a broad smooth maximum

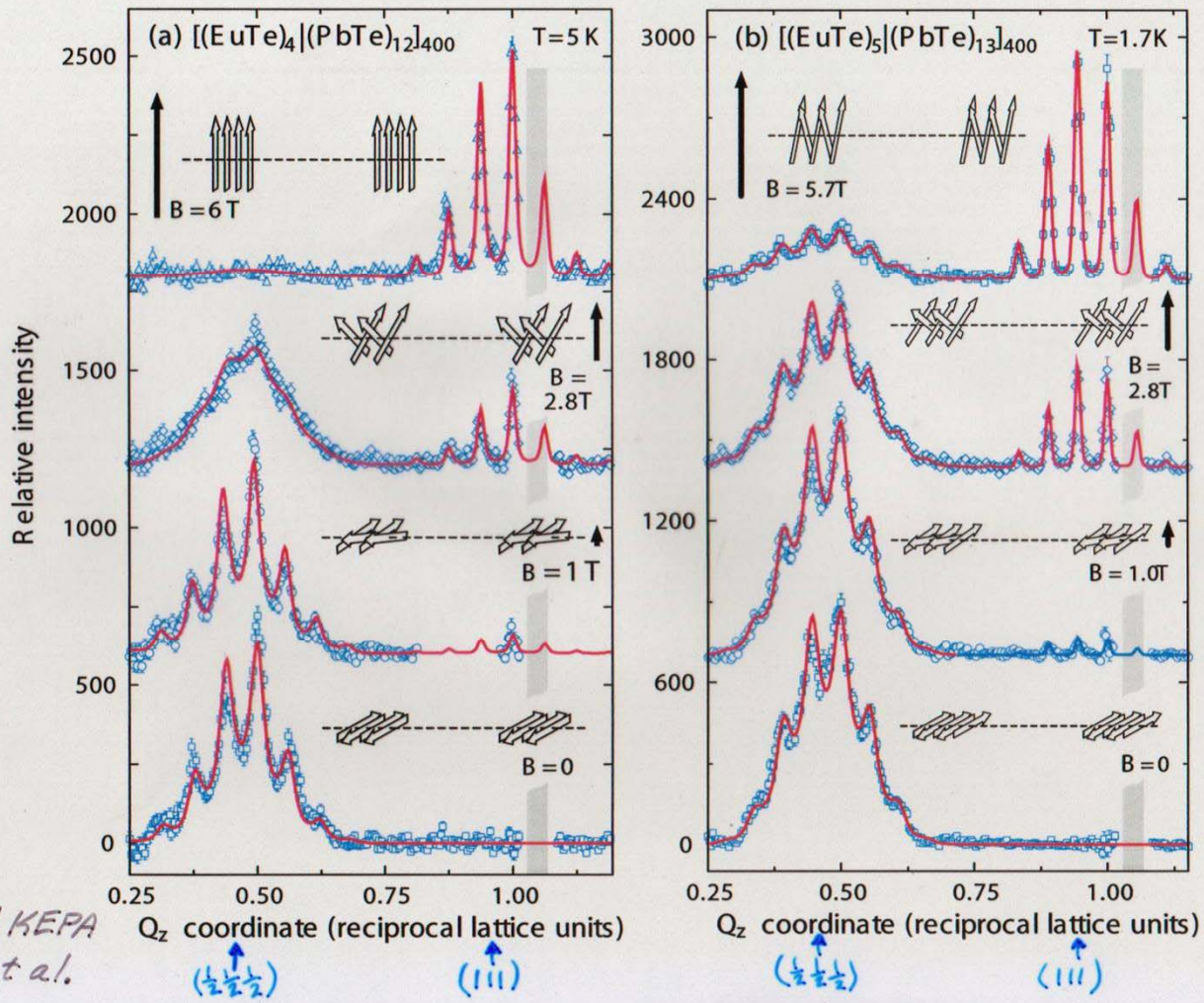
(a) [(EuTe)4|(PbTe)12]400
T=5 K
B = 6 T
B = 2.8T
B = 1 T
B = 0
(b) [(EuTe)5|(PbTe)13]400
T=1.7K
B = 5.7T
B = 2.8T
B = 1.0T
B = 0
Relative intensity
Qz coordinate (reciprocal lattice units)
0.25
0.50
0.75
1.00
(½½½)
(111)

H. KEPA et al.

Pinpointing Chiral Structures with Front/Back Polarized Neutron Reflectometry

We have developed a new method of using polarized neutron reflectometry (P N R) to extract the structure of buried magnetic spirals in magnetic films. This technique improves upon earlier methods by being particularly sensitive to the presence of magnetic twists vis-à-vis structures in which the magnetization direction does not vary appreciably. Tracking the formation and growth of twists may solve a number of puzzles that hamper the development of magnetic thin film devices.

In collaboration with I B M scientists, we have applied the technique to a thin-film exchange-spring magnet and confirmed that the results may violate the current theory regarding the behavior of such magnets. It has been predicted that exchange-spring magnets, comprised of soft and hard ferromagnets in close proximity, are a composite that has a strong moment and does not readily demagnetize (Refer to Reference 1). Therefore, exchange-spring magnets should give industry the ability to make much smaller permanent magnets for use in the magnetic recording devices, and elsewhere. As a side effect, when a small external magnetic field is opposed to that of the magnet, the portion of the soft ferromagnet farthest from the hard ferromagnet may twist into alignment with the field. When the field is removed, the soft ferromagnet untwists. The film provided by I B M consists of the hard ferromagnet $Fe_{55}Pt_{45}$ topped by the soft ferromagnet $Ni_{80}Fe_{20}$ (Refer to Reference 2).

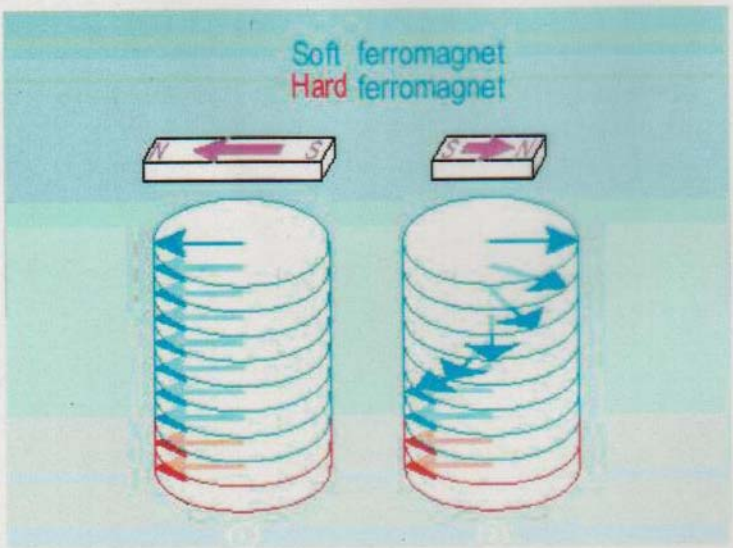

FIGURE 1. Model for field behavior of exchange-spring magnets. On the left the magnet has been aligned by a large external magnetic field. On the right a smaller field opposed to the

first field causes a twist to form in the soft ferromagnet, while the hard ferromagnet remains aligned.

Figure 1 shows a simplified diagram of the behavior predicted by current theories (Refer to Reference 1). A magnetic field of 0.890 T, provided by an electromagnet, is sufficient to align both the soft and the hard layers of our exchange-spring magnet, as shown on the left. When a modest reverse field (on the order of 0.025 T) is applied to the exchange spring magnet, only the top of the soft layer will realign with the magnetic field. The hard layer remains pinned in the original direction, and a continuous twist is induced in the soft layer, as the direction of magnetization changes smoothly between the reverse field direction to the aligning field direction.

Although there are many alternatives to P N R to measure the magnetization, typically they measure only the average orientation of the magnetic spins, and cannot readily distinguish a spiral from a structure in which all the spins are canted with respect to an external field. P N R can extract the depth-dependence of the magnetic and chemical structure. We have studied the sample over a wide range of external magnetic fields, and can track the development of the spiral with field (Refer to Reference 3).

A P N R experiment begins with neutrons whose magnetic moments are aligned parallel (+) or opposite (-) to the external magnetic field. When the magnetization of the sample is perpendicular to this magnetic field, the neutron moment precesses as it interacts with the sample. When this happens the spin-flip (S F) reflectivities R^{+-} and R^{-+} are strong. If the magnetization of the sample is parallel to the external magnetic field, no precession occurs, but the non-spin-flip (N S F) reflectivities R^{++} and R^{--} will differ. The N S F reflectivities also provide information about the chemical structure of the film.

Our new modification of the P N R method greatly enhances the contrast between colinear and certain non-colinear magnetic structures (Refer to Reference 4). We first measure the reflectivity with neutrons glancing off the front surface of the material, and then repeat with neutrons glancing off the back surface. The experiment is akin to holding the plane of the film up to a ?magnetic mirror? to see whether the mirror image is the same as the original structure. In a colinear structure, all the spins are aligned along a common direction, and the mirror image is very much like the original structure. But the mirror image of a magnetic twist to the right is a magnetic twist to the left. Therefore, if the front and back reflectivities are significantly different, we can deduce the presence of a spiral. Fitting the data confirms the spiral?s existence.

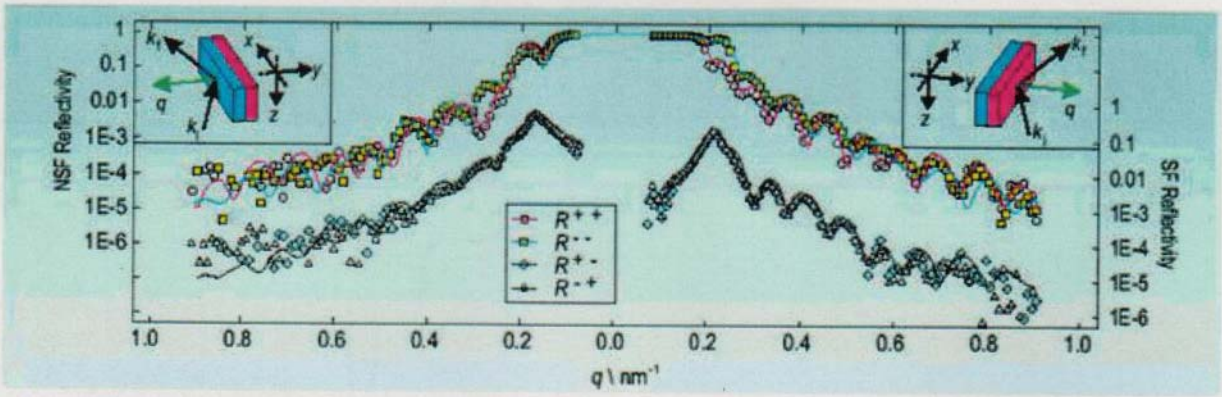

FIGURE 2. Reflectivity of a $Ni_{80}Fe_{20}$ | $Fe_{55}Pt_{45}$ bilayer. The front reflectivity is plotted on the right while the back reflectivity is plotted on the left. The S F reflectivities R^{+-} and R^{-+} are plotted against the right ordinate axis. The NSF reflectivities R^{++} and R^{--} are plotted against the left ordinate axis.

Figure 2 shows data collected at 0.026 T after aligning in -0.89 T. Fits to the data are shown as solid lines. The data from the front reflectivity are shown on the right, and the data from the back reflectivity are shown on the left. The spin-flip (S F) reflectivities R^{+-} and R^{-+} are plotted against the right-hand axis, which have been shifted relative to the N S F reflectivities R^{++} and R^{--} plotted against the left axis. At $q = 0.2\ nm^{-1}$, there is a splitting in the front N S F reflectivity that is much more pronounced than that of the back reflectivity at the same q. This is a hallmark of the spiral structure.

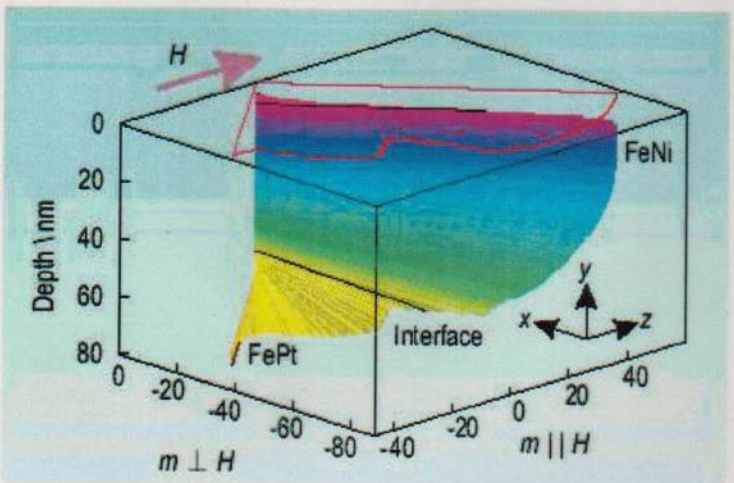

FIGURE 3. Fitted magnetization of the data presented in Figure 2. The front of the sample is at a depth of 0 nm and the back is at a depth of 70 nm. The red curve is a projection of the magnetic structure into the plane of the front surface.

Figure 3 shows the magnetic structure that gives the excellent fit to the data plotted in Figure 2. The location of the hard / soft interface is marked in Figure 3. Surprisingly, we discover the spiral invades the hard ferromagnet even at extremely low fields. Current theory predicts that when this occurs, the soft ferromagnet will not be able to untwist fully. Yet, other

magnetic studies show that our exchange-spring magnet does untwist when this field is removed. Thus, our P N R measurements have identified a shortcoming of current theory.

With this new technique, N I S T is now able to better characterize the magnetic properties of thin films, which can improve the capability and reliability of industrial devices for magnetic recording and sensing.

References

[1] E. F. Kneller and R. Hawig, I E E E Trans. Magn. 27, 3588 (1991).
Online Verison of the article

[2] O. Hellwig, J. B. Kortright, K. Takano, and E. E. Fullerton, Phys. Rev. B62, 11694 (2000).
Online version

[3] K. V. O?Donovan, J.A. Borchers, C.F. Majkrzak, O. Hellwig and E.E. Fullerton. Physical Review Letters 88, 067201 (2002)
Online Version

[4] K. V. O?Donovan, J.A. Borchers, C.F. Majkrzak, O. Hellwig and E.E. Fullerton. Applied Physics A 74 [Suppl.], S1544 (2002)
Online Version

Authors

K. V. O?Donovan, J. A. Borchers, and C. F. Majkrzak
N I S T Center for Neutron Research
National Institute of Standards and Technology
Gaithersburg, MD 20899-8562

O. Hellwig, E. E. Fullerton
I B M Almaden Research Facility
San Jose, CA 95120-6001

Back to Reflectometry Scientific Highlights

Last modified 27-January-2003

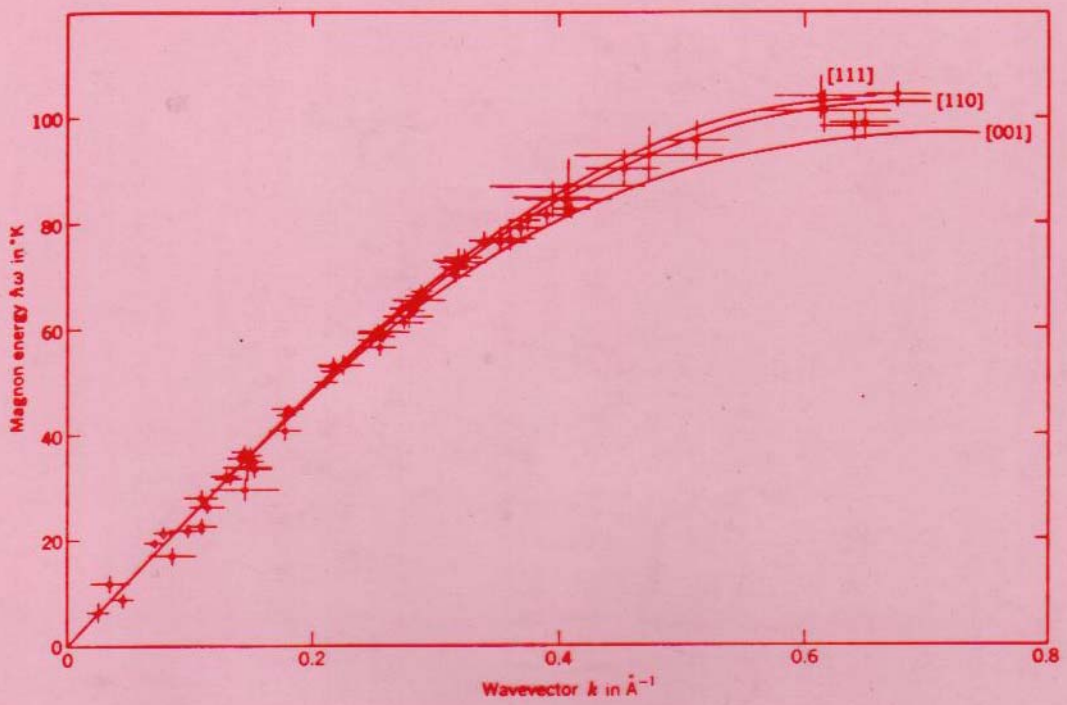

Figure 29 Magnon dispersion relation in the simple cubic antiferromagnet $RbMnF_3$ as determined at 4.2°K by inelastic neutron scattering. The observed points are for wavevectors anywhere in a (110) plane; the curves are calculated in three indicated directions for a nearest neighbor exchange interaction $J/k_B = 3.4$°K. [After C. G. Windsor and R. W. H. Stevenson, Proc. Phys. Soc. (London) 87, 501 (1966).]

(KITTEL)

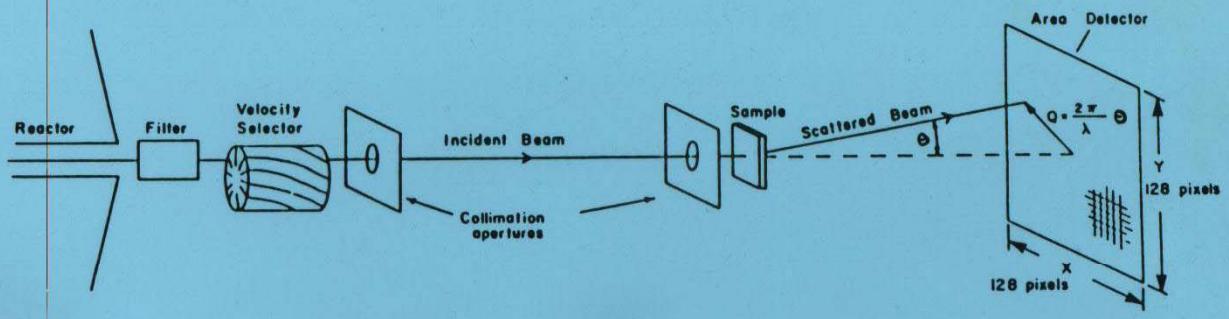

Small Angle Neutron Scattering (SANS) probes structure

on a scale d where

$$d \approx \frac{2\pi}{Q} \qquad Q = k_i - k_f$$

$$d \approx \frac{\lambda}{\theta} \quad \begin{matrix}\text{(wavelength)} \\ \text{(scattering angle)}\end{matrix} \qquad Q = \frac{4\pi}{\lambda} \sin(\theta/2)$$

$5\ \text{Å} < \lambda < 20\ \text{Å}$ (cold neutrons)

$0.1^\circ < \theta < 10^\circ$

$10\ \text{Å} < d < 5000\ \text{Å}$

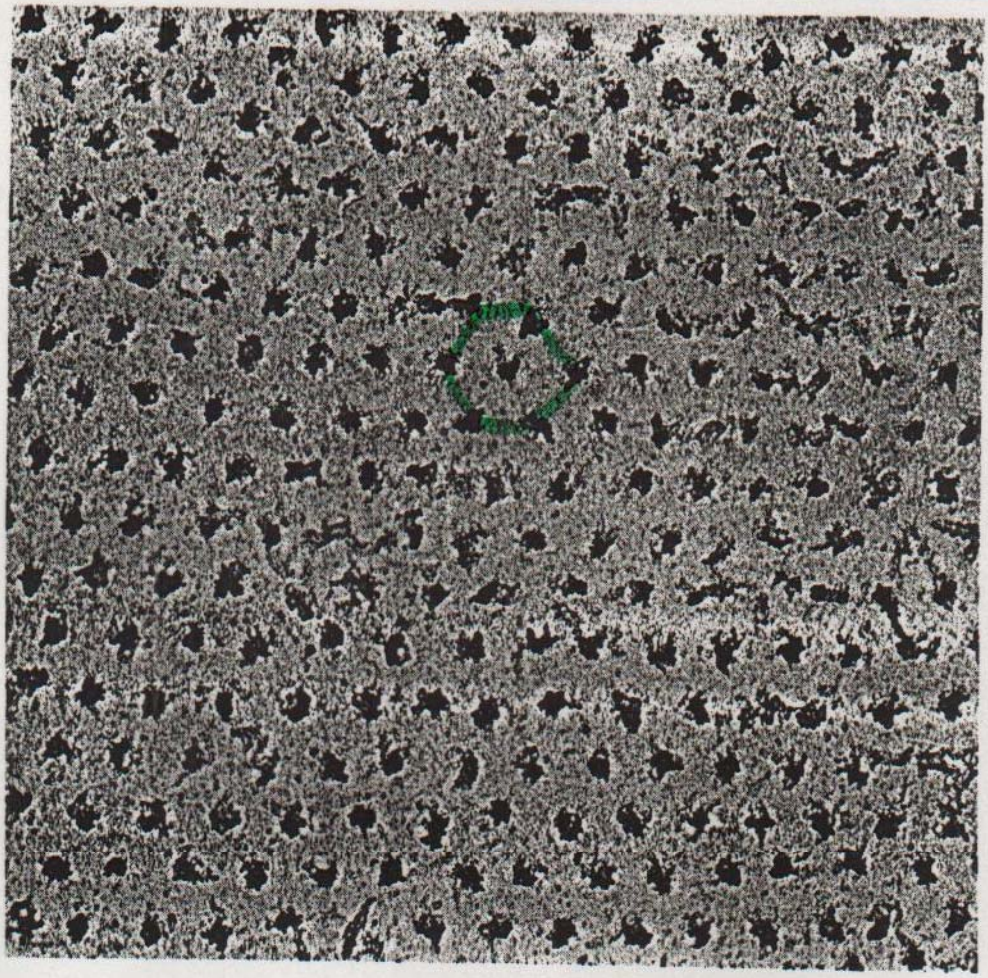

Figure 37 Triangular lattice of flux lines through top surface of a superconducting cylinder. The points of exit of the flux lines are decorated with fine ferromagnetic particles. The electron microscope image is at a magnification of 8300.-(Courtesy of U. Essmann and H. Träuble.)

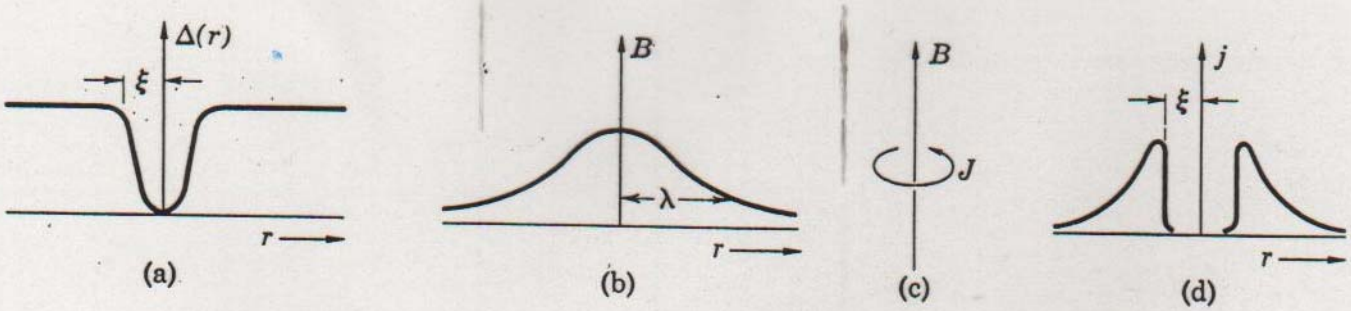

FLUXOID LATTICE

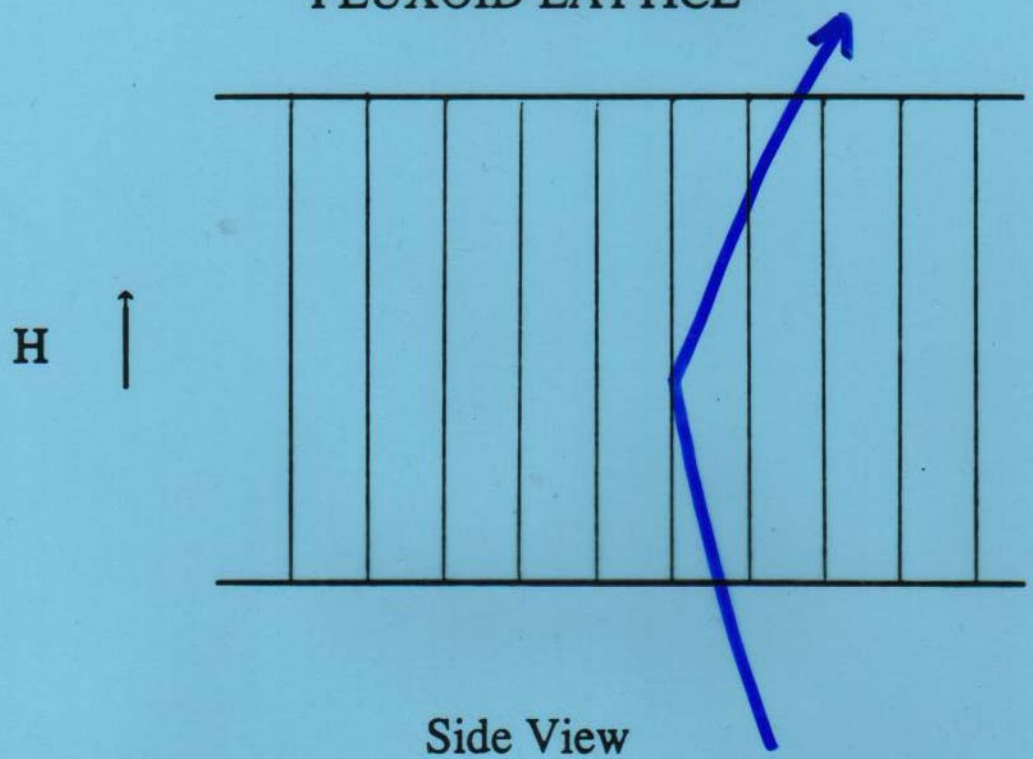

Side View

$$\frac{\lambda}{2d} = \frac{n}{} = \sin\theta \approx \theta$$

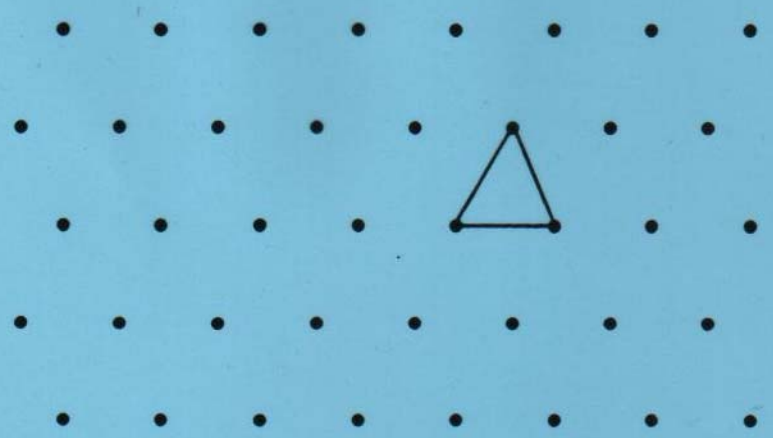

Top View

Nb

Counting time ~2 minutes

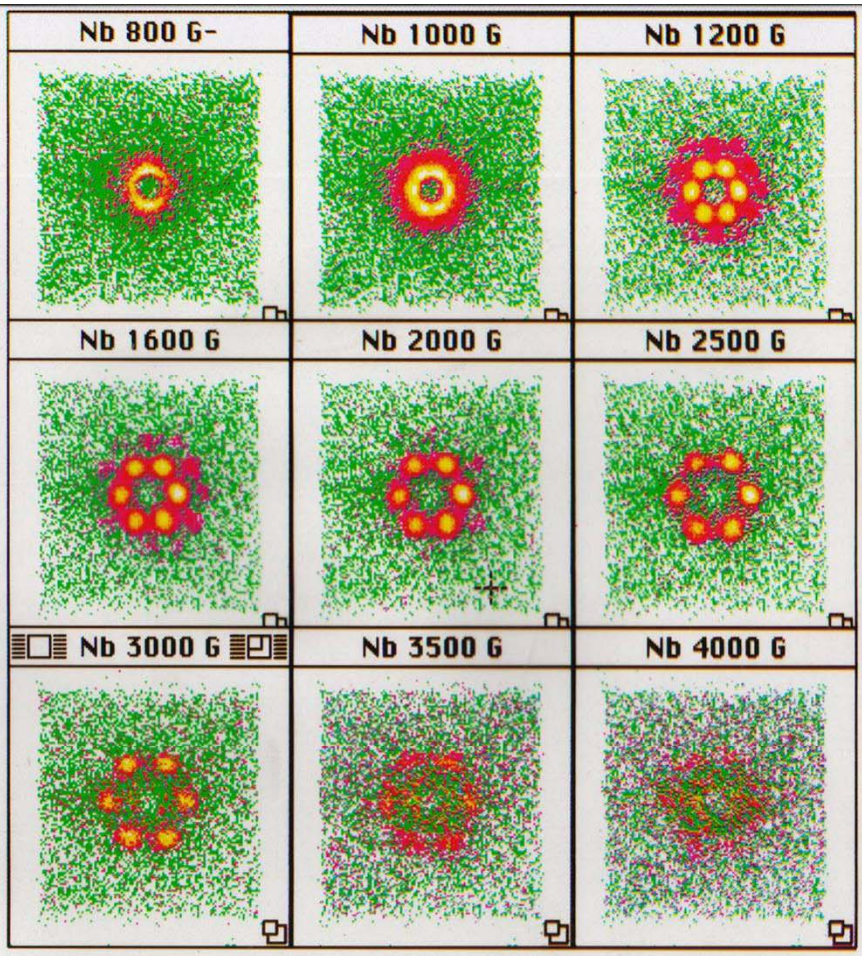

$T \approx 4.4\,K$

Vortex Lattice Dynamics in Niobium

J.W. Lynn, et al, Phys. Rev. Lett. 72, 3413 (1994)